FBN-1, a fibrillin-related protein, is required for resistance of the epidermis to mechanical deformation during *C. elegans* embryogenesis

Melissa Kelley, John Yochem, Michael Krieg, Andrea Calixto, Maxwell G Heiman, Aleksandra Kuzmanov, Vijaykumar Meli, Martin Chalfie, Miriam B Goodman, Shai Shaham, Alison Frand, David S Fay

DOI: http://dx.doi.org/10.7554/eLife.06565

Cite as: eLife 2015;10.7554/eLife.06565

Received: 19 January 2015
Accepted: 20 March 2015
Published: 23 March 2015

FBN-1, a fibrillin-related protein, is required for resistance of the epidermis to mechanical deformation during *C. elegans* embryogenesis

Melissa Kelley[1a], John Yochem[1a], Michael Krieg[2,3a], Andrea Calixto[4,5], Maxwell G. Heiman[6], Aleksandra Kuzmanov[1], Vijaykumar Meli[8], Martin Chalfie[4], Miriam B. Goodman[2], Shai Shaham[7], Alison Frand[8], and David S. Fay[1]*

[1]Department of Molecular Biology, University of Wyoming, Laramie, WY, USA

[2]Department of Molecular and Cellular Physiology, Stanford University, Stanford, CA, USA

[3]Department of Chemical Engineering, Stanford University, Stanford, CA, USA.

[4]Department of Biological Sciences, Columbia University, New York, NY, USA

[5]Center for Genomic and Bioinformatics, Universidad Mayor, Santiago, Chile

[6]Department of Genetics, Harvard Medical School and Division of Genetics, Boston Children's Hospital, Boston, MA, USA

[7]Laboratory of Developmental Genetics, The Rockefeller University, New York, NY, USA

[8]Department of Biological Chemistry, David Geffen School of Medicine, University of California, Los Angeles, CA, USA

Running Title: *C. elegans fbn-1*

Key words: *C. elegans*, embryogenesis, biomechanical forces, splicing, fibrillin

[a]Co-first authors

*Corresponding author: Dept. 3944, 1000 E. University Avenue, Department of Molecular Biology, College of Agriculture and Natural Resources, University of Wyoming, Laramie, WY 82071; Telephone: (307) 766-4961; Fax: (307) 766-5098 email: davidfay@uwyo.edu

COMPETING INTERESTS

The authors of this manuscript have no competing interests as defined by the International committee of Medical Journal Editors.

ABSTRACT (150 words: 150 allowed)

During development, biomechanical forces contour the body and provide shape to internal organs. Using genetic and molecular approaches in combination with a FRET-based tension sensor, we characterized a pulling force exerted by the elongating pharynx (foregut) on the anterior epidermis during *C. elegans* embryogenesis. Resistance of the epidermis to this force and to actomyosin-based circumferential constricting forces is mediated by FBN-1, a ZP domain protein related to vertebrate fibrillins. *fbn-1* was required specifically within the epidermis and FBN-1 was expressed in epidermal cells and secreted to the apical surface as a putative component of the embryonic sheath. Tiling array studies indicated that *fbn-1* mRNA processing requires the conserved alternative splicing factor MEC-8/RBPMS. The conserved SYM-3/FAM102A and SYM-4/WDR44 proteins, which are linked to protein trafficking, function as additional components of this network. Our studies demonstrate the importance of the apical extracellular matrix in preventing mechanical deformation of the epidermis during development.

INTRODUCTION

In addition to their essential protective, structural and physiological functions, epithelial cells and their closely associated extracellular matrices (ECMs) serve as important mediators of embryonic morphogenesis and organogenesis (Davidson, 2011; Davidson, 2012; Heisenberg and Bellaiche, 2013). These developmental functions require epithelial tissues to be appropriately resistant to deformation by a variety of intrinsic and extrinsic mechanical forces that arise during the normal course of development. Accordingly, an improper force balance can lead to morphological abnormalities and birth defects (Epstein et al., 2004; Moore et al., 2013).

In *Caenorhabditis elegans*, the outermost epithelial layer or epidermis (commonly called the hypodermis in nematodes) is initially established during early-to-mid embryogenesis (~400 min post fertilization; Sulston et al., 1983). At this time, future epidermal cells execute stereotypical movements, shape changes and migrations to produce a 1.5-fold-stage embryo that is surrounded by an epithelium consisting of a single cell layer (Chisholm and Hardin, 2005; Chisholm and Hsiao, 2012; Sulston et al., 1983). Shortly after this stage, ring-shaped actomyosin bundles, which are spaced regularly along the anteroposterior axis of the embryo, undergo coordinated contraction. This contraction leads to the circumferential constriction of the embryo and its conversion to a tapered cylindrical (fusiform) shape that is ~250 μm long (about five times the length of the egg shell; Costa et al., 1997; Priess and Hirsh, 1986). As a consequence of constriction at the epidermal surface and contractions by body wall muscles (Chisholm and Hardin,

2005; Williams and Waterston, 1994), tissues and organs inside the embryo are thought to experience squeezing forces and to elongate in conjunction with the outer layers of the embryo. Notably, the apical ECM (aECM) of the embryonic epidermis, termed the embryonic sheath, is required to prevent excessive constriction and deformation of the epidermis by actomyosin ring contraction (Priess and Hirsh, 1986). Although critical for development, the molecular composition and related physical properties of the embryonic sheath remain poorly characterized.

Despite a growing interest in mechanical aspects of development and morphogenesis (Guillot and Lecuit, 2013; Heisenberg and Bellaiche, 2013), the interplay between mechanical forces and the physical properties and structure of tissues have been difficult to characterize. This is due in part to an incomplete description of mechanical forces in living embryos. In addition, genetic redundancy has likely impeded progress toward fully understanding the molecular control of tissue and organismal morphogenesis (Bussey et al., 2006; Herman and Yochem, 2005; Pickett and Meeks-Wagner, 1995; Tautz, 2000; Thomas, 1993).

Here we describe a morphological defect that results from the failure of the anterior epidermis to maintain its proper shape while experiencing an inward-directed pulling force exerted by the developing pharynx (foregut) as it undergoes elongation. This defect occurs at a low frequency in single mutants of *mec-8*, *sym-3* and *sym-4*, but at a high frequency in *mec-8; sym-3* and *mec-8; sym-4* double mutants, indicating that this

process is redundantly controlled (Davies et al., 1999; Yochem et al., 2004). Whereas *sym-3* and *sym-4* encode conserved proteins with predicted roles in vesicular trafficking (Yochem et al., 2004; also see Discussion), *mec-8* encodes a conserved RNA-binding protein involved in alternative splicing (Lundquist et al., 1996; Spike et al., 2002). We have shown that the contribution of MEC-8 in the resistance to this force arises, at least in part, through its control of FBN-1, a protein that shares several domains with vertebrate fibrillins and acts in the embryonic sheath. Notably, mutations in human fibrillin genes lead to connective tissue disorders including Marfan syndrome (Dietz et al., 2005; Ramirez and Dietz, 2009; Ramirez and Sakai, 2010).

RESULTS

Morphological defects in *mec-8; sym-3* and *mec-8; sym-4* mutants are caused by an inward-directed pulling force exerted by the pharynx on the epidermis.

In wild-type embryos at the 1.5-fold stage of development, a shallow pit (~2.1 μm deep), termed the sensory depression, is detected in the region corresponding to the location of the future mouth (buccal cavity; Figure 1A, Table 1; Sulston et al., 1983). This morphological feature is relatively short-lived and is no longer visible in 3-fold-stage embryos (Figure 1A, Figure 2C). In contrast, *mec-8; sym-3* and *mec-8; sym-4* embryos had a striking keyhole-shaped invagination in this region, which increased in depth between the 1.5- (~4.3 μm) and 3-fold (~9.5 μm) stages (Figure 1A, Table 1). In contrast to wild-type L1 larvae, in which the pharynx and associated buccal capsule (terminal mouth part) extended to the anterior tip of the worm, *mec-8; sym-3* and *mec-8; sym-4* L1 larvae displayed what we have termed the "Pharynx ingressed" (Pin) phenotype, in which the pharynx and buccal capsule are displaced toward the posterior end of the animal (Figure 1A). In Pin larvae, lateral anterior tissues appeared to fold over and surround the ingressed buccal capsule, thereby preventing double mutants from feeding (Figure 1A). Although these defects were observed at only low frequencies in *sym-3*, *sym-4* and *mec-8* single mutants, they were highly penetrant in *mec-8; sym-3* and *mec-8; sym-4* double mutants (Figure 1B, Supplementary File 1).

To account for the defects observed in *mec-8; sym-3* and *mec-8; sym-4* double mutants, we proposed a testable model for pharyngeal and embryonic elongation. As

described above, the embryo acquires an elongated shape through the circumferential constriction of ring-shaped actomyosin bundles arrayed along the surface of the epidermis (Priess and Hirsh, 1986). During initial stages of embryonic morphogenesis (~350–380 min), the primordial pharynx exists as a ball of cells with no connection to the future mouth (buccal capsule) or epidermis (Figure 1C). Linkage of the pharynx to the mouth and epidermis is established between the comma and 1.5-fold stages (~380–410 min; Figure 1C, data not shown; (Portereiko and Mango, 2001; Sulston et al., 1983). During embryonic development, the pharynx lengthens along its anteroposterior axis, transforming from a blunt conical shape into a bi-lobed structure that is attached to the mouth at the anterior and to the intestine in the mid body (Figure 1C). We hypothesized that lengthening of the pharynx is facilitated in part by an outward-directed pulling force that is exerted by the anterior epidermis as the embryo undergoes elongation. In addition, as the pharynx is stretched, it exerts a counter inward-pulling force on the embryonic epidermis. This inward-pulling force would be greatest in the region where the pharynx attaches to the epidermis, contributing to the formation of the sensory depression (Figure 1C). We liken this situation to that of a spring that is attached (on the inside) to the “anterior” end of an elastic-walled cylinder, with the cylinder representing the embryonic epidermis and the spring representing the pharynx (Figure 1C). The “posterior” end of the spring in this model is held in place within the middle of the cylinder through localized contacts, which in the case of the pharynx most likely occur through cell-cell interactions. As the cylinder elongates, it stretches the spring, which then exerts an inward-pulling force at the site of attachment to the cylinder

148 wall (Figure 1C). We hypothesize that in wild-type embryos, one or more means of
149 structural reinforcement prevents the anterior epidermis from undergoing a pronounced
150 invagination or ingression in response to the pharyngeal pulling force. In contrast, the
151 epidermis in *mec-8; sym-3* and *mec-8; sym-4* mutants is insufficiently reinforced, due to
152 the combined defects in processes controlled by *mec-8* and *sym-3/4*, resulting in
153 mechanical deformation of the epidermis, the genesis of the keyhole and, ultimately, the
154 Pin phenotype.
155
156 One prediction of our model is that prevention of a pharyngeal-epidermal attachment
157 should suppress keyhole formation in *mec-8; sym-3/4* embryos (Figure 2A). To test this,
158 we used a deletion mutation (*tm3671*) in *pha-1*, which encodes a cytoplasmic protein of
159 unknown function, that prevents initial attachment of the pharynx to the epidermis in
160 ~85% of embryos (Fay et al., 2012; Fay et al., 2004; Kuzmanov et al., 2014). As
161 predicted, formation of the keyhole was suppressed in *mec-8; pha-1(tm3671); sym-3*
162 triple mutants in which the pharynx failed to attach (Figure 2A, Table 1). In contrast, in
163 *mec-8; pha-1(tm3671); sym-3* embryos in which the pharynx was attached to the
164 epidermis (~15%), a keyhole was observed, indicating that the loss of attachment per
165 se, rather than the loss of *pha-1* activity, was responsible for the suppression of keyhole
166 formation in the majority of triple mutants (Figure 2A).
167
168 A second prediction of our model is that maintenance of a pharyngeal-epidermal
169 attachment would be required for persistence of a keyhole in embryos and for

progression to a Pin phenotype in larvae (Figure 2B). To test this prediction, we used a hypomorphic allele of *pha-1* (*e2123*), which establishes a transient connection between the pharynx and epidermis that is severed at later stages of embryogenesis (Fay et al., 2004; Kuzmanov et al., 2014; Schnabel and Schnabel, 1990). In our cylinder-and-spring analogy, loss of the pharyngeal-epidermal attachment in *pha-1(e2123)* mutants would be akin to severing the spring near the site of attachment to the tube, leading to the ingressed elastic cylinder tip popping back out and recoil of the spring (Figure 2B). As predicted by our model, early-stage *mec-8; pha-1(e2123); sym-3* triple mutants formed a stereotypical keyhole, consistent with the presence of a pharyngeal-epidermal connection. The absence of a keyhole or Pin phenotype in late-stage embryos and L1 larvae, however, indicated that anterior ingression of the epidermis requires a sustained pulling force exerted by the pharynx and that the keyholes are not static once formed (Figure 2B).

We also observed that the depth of the keyhole in *mec-8; sym-3* and *mec-8; sym-4* mutants steadily increased from the comma stage to the 3-fold stage of embryogenesis (Figure 1A, Figure 2C, Table 1). We hypothesized that failure to elongate past the 1.5- or 2.0-fold stages would, however, prevent further deepening of the keyhole. In our model, this would be akin to lengthening the cylinder only partway, thereby preventing further ingression of the tip. To test this, we inhibited morphogenesis past the 2-fold stage in *mec-8; sym-4* mutants by RNA interference (RNAi) of *let-502/ROCK*, which encodes an epidermal-expressed Rho-binding kinase required for embryonic elongation

192 (Wissmann et al., 1999; Wissmann et al., 1997). As expected, keyhole depth in *mec-8;*
193 *sym-4; let-502(RNAi)* embryos increased until the 2-fold stage, reaching an average
194 depth of ~6 μm, identical to that observed for control RNAi-treated *mec-8; sym-4*
195 mutants at the same stage of development (Figure 2C). After morphogenetic arrest,
196 however, keyholes in *mec-8; sym-4; let-502(RNAi)* embryos failed to deepen, indicating
197 that the progressive increase in keyhole depth is a function of embryonic elongation,
198 rather than the passage of time. We also observed that *mec-8; sym-4; let-502(RNAi)*
199 embryos took longer to transit from the comma stage to the 2-fold stage than the control
200 RNAi-treated strain. Consistent with our model, the rate at which keyhole depth
201 increased in *mec-8; sym-4; let-502(RNAi)* embryos was reduced in proportion with the
202 delay in embryonic elongation (Figure 2C).
203
204 A final prediction of our model is that a reversal of embryonic elongation should lead to
205 a consequent reduction in the depth of the keyhole in embryos. In our model, this would
206 be analogous to shortening the cylinder and observing a reduction in anterior tip
207 ingression (Figure 2D). To test this, we used a conditional allele of *sqt-3* (*e2117ts*),
208 which undergoes a reversal of elongation from the ~3-fold to ~2-fold stages after
209 temperature upshift (Kusch and Edgar, 1986; Priess and Hirsh, 1986). Consistent with
210 our model, keyholes reached a maximum depth of ~8–10 μm at around the 3-fold stage
211 but then shrunk to ~4–6 μm after a partial reversal of embryonic elongation (Figure 2D).
212 Taken together, our findings provide strong evidence that resistance of the pharynx to
213 stretching or lengthening leads to an inward-pulling force on the anterior epidermis

during much of embryogenesis. In the case of wild-type embryos, this force is resisted to an appropriate extent, and a normal morphology is achieved. In contrast, morphological defects in *mec-8; sym-3* and *mec-8; sym-4* embryos and larvae suggest that the mechanical properties of the epidermis may be compromised in these mutants, leading to the Pin phenotype.

A FRET-based tension sensor reveals mechanical forces operating during embryogenesis.

To visualize biomechanical forces operating during embryogenesis, we made use of recently developed FRET-based methods for detecting mechanical tension in live cells (Grashoff et al., 2010; Meng et al., 2011; Meng et al., 2008). Specifically, we used strains expressing a tension sensor module (TSMod) inserted into the coding sequence of the *unc-70* gene (Figure 3A; (Krieg et al., 2014). UNC-70, a β-spectrin ortholog, is expressed widely during embryogenesis and acts together with α-spectrin and actin to form a subcortical cytoskeletal network that is critical for cell shape and mechanics in a variety of cell types in *C elegans* (Bretscher, 1991; Hammarlund et al., 2000; Moorthy et al., 2000; Norman and Moerman, 2002). Importantly, the UNC-70(TSMod) fusion protein localized to the cell membrane cortex in a pattern that was seemingly identical to immunostaining of endogenous UNC-70 (Moorthy et al., 2000), with a prominent accumulation at future location of the buccal cavity (Figure 3B). Moreover, UNC-70(TSMod) rescued the severely paralyzed locomotion phenotype of *unc-70* null mutant animals, indicating that the fusion protein is functional (Krieg et al., 2014).

The TSMod sensor consists of a donor (mTFP) and acceptor (Venus) fluorophore separated by a flexible linker made of 40 residues from the spider-silk flagelliform, which acts as an entropic nanospring suitable for estimating biologically relevant forces (Figure 3A; Grashoff et al., 2010). The linker is sensitive to molecular forces in various systems (Borghi et al., 2012; Cai et al., 2014; Krieg et al., 2014; Morimatsu et al., 2013; Paszek et al., 2014). Thus, as stretching forces act on this spring the two FRET fluorophores will be pulled apart and lead to a visible change in energy transfer. Consequently, a low FRET index indicates the application of a stretching force to UNC-70(TSMod) and suggests that actin-spectrin networks in such regions experience high levels of mechanical tension. Conversely, a high FRET index suggests that such regions experience low or no tension across the actin-spectrin network. Importantly, we previously used this same sensor to investigate mechanical tension in *C. elegans* neurons and extend this robust imaging procedure (see Methods) to characterize its performance in living animals (Krieg et al., 2014).

To quantify the extent to which pharyngeal attachment and subsequent pulling forces lead to higher tension near the sensory depression, we compared FRET at the sensory depression region (SDR) with areas outside the sensory depression (non-SDR) in embryos before and after pharyngeal attachment to the epidermis (early comma and 1.5-fold stages, respectively; see Methods). This strategy allows us to compare pixels from the SDR and non-SDR that have been measured under exactly the same

conditions in a pairwise manner, since both measurements were derived from the same image and analyzed identically. Thus, any changes in FRET efficiency are unlikely result from differences in expression levels of the sensor or imaging conditions. No significant differences in UNC-70(TSMod) FRET efficiency were observed between the sensory depression region (SDR) and non-SDR region prior to the attachment of the pharynx to the epidermis (early comma stage) in either wild-type or *pha-1(0)* embryos (Figure 3E,I). In contrast, wild-type 1.5-fold embryos had significantly higher tension (lower FRET) at the SDR as compared with regions outside the sensory depression ($P=0.0008$), consistent with the hypothesis that pharyngeal attachment contributes to the force balance at the sensory depression (Figure 3C,D,I; Supplementary File 2). In contrast, 1.5-fold *pha-1(0)* mutants in which the pharynx failed to attach did not display appreciably lower levels of mechanical tension at the SDR as compared with regions outside the sensory depression ($P=0.2421$; Figure 3G,H,I; Supplementary File 2). In addition, tension at the SDR was significantly higher in wild-type embryos as compared with the SDR region in *pha-1(0)* mutants at the 1.5-fold ($P<0.0001$) but not early comma stages ($P=1.000$; Supplementary File 2), also consistent with pharyngeal attachment and pulling leading to tension at the anterior epidermis.

To interpret UNC-70(TSMod) FRET signals during early stages of embryogenesis, we replaced the flexible linker by a large separator (TRAF) or a short linker of only five residues (5aa) to generate UNC-70(TRAF) and UNC-70(5aa) constructs in which the two FRET fluorophores are separated by a constant distance and, importantly, are

insensitive to force. As expected, both control sensors localized in a pattern that was indistinguishable from endogenous UNC-70 (data not shown; Moorthy et al., 2000), rescued the paralyzed phenotype of *unc-70* adults (data not shown; see Methods), and showed FRET values consistent with the distance of the fluorophores (Figure 3 – Figure supplement 1). In addition, no significant differences were observed between SDR and non-SDR regions in 1.5-fold wild-type embryos using these controls (Figure 3 – Figure supplement 1; Supplementary File 2) and their FRET efficiency values are similar to those reported previously (Borghi et al., 2012; Krieg et al., 2014).

To further confirm that the observed differences in the FRET efficiency of UNC-70(TSMod) reliably report differences in molecular tension in our experimental system, we generated animals that carry an UNC-70(N-TSMod) fusion protein, in which the force sensitive FRET construct has been placed at the N-terminus of full-length unc-70 β-spectrin. In this position, the TSMod is not responsive to force and would be predicted to yield FRET signatures consistent with no-force situations. Similar the other UNC-70 fusion proteins, UNC-70(N-TSMod) was expressed in a pattern indistinguishable to that of the native UNC-70 protein and the transgene restored locomotion to paralyzed *unc-70* adult animals (data not shown). As expected, FRET values were higher in embryos that expressed the force-insensitive UNC-70(N-TSMod) versus UNC-70(TSMod) (Figure 3; Supplementary File 2), consistent with previous results that a terminal TSMod fusion cannot be pulled apart by cellular forces (Borghi et al., 2012; Conway et al., 2013; Grashoff et al., 2010; Krieg et al., 2014). Importantly, we did not see gross

variations in FRET across different tissues within the same embryo in N-TSMod expressing animals, consistent with the idea that the variation in UNC-70(TSMod) is due to different forces acting on UNC-70. We also noted that FRET values were independent of the expression level of the fluorophores, indicating that the FRET signal in each pixel was predominantly coming from intramolecular as opposed to intermolecular energy transfer (data not shown). Taken together, the FRET tension sensor provides strong independent support for our model in which the anterior epidermis experiences a high level of mechanical stress that is due in large part to forces exerted by the pharynx (Figure 1C).

MEC-8 regulates the splicing of FBN-1, a fibrillin-like protein.

We hypothesized that MEC-8, an RNA-binding protein and known splicing factor (Calixto et al., 2010; Lundquist et al., 1996; Spike et al., 2002), may regulate the mRNA processing of one or more genes that function to stabilize the epidermis in response to mechanical forces. Because the RNA recognition site for MEC-8 is unknown, we used a non-biased approach to identify candidate MEC-8 targets. mRNAs obtained from wild-type and *mec-8* mutant embryos were analyzed using a whole-genome tiling-array approach (He et al., 2007; Mockler et al., 2005). We identified 1,106 individual regions within a total of 449 genes that were differentially expressed (>1.5-fold) between wild-type and *mec-8* embryos (Supplementary Files 3,4). This included 159 genes (666 regions) in which at least one exon was upregulated in *mec-8* mutants, 286 genes (421

regions) in which at least one exon was downregulated in *mec-8* mutants and 12 genes (19 regions) in which at least one intron was upregulated in *mec-8* mutants (Supplementary Files 3,4). We note that seven genes included in the totals above contained both upregulated introns and exons. Among the 449 identified genes, 135 (30%) are annotated by WormBase as having multiple (alternatively spliced) isoforms (Supplementary Files 3,4). This included 67% (8/12) of the genes with up-regulated introns, 47% (75/159) of genes with up-regulated exons and 22% (52/286) of genes with down-regulated exons. Tiling-array findings were confirmed for several genes within each of the categories described above by PCR analysis (Figure 4–figure supplement 1; Supplementary Files 3,4).

Many of the identified genes, particularly those with only a single identified mRNA isoform, are unlikely to be direct targets of MEC-8, which regulates alternative splicing (Calixto et al., 2010; Spike et al., 2002). Such genes are more likely to display transcriptional misregulation as an indirect consequence of *mec-8* loss. Also, a significantly higher proportion of the identified genes containing either up-regulated exons or introns were alternatively spliced, as compared with genes containing down-regulated exons ($P < 0.0001$ and $P < 0.005$, respectively) or in comparison with all annotated *C. elegans* genes ($P < 0.0001$ and $P < 0.005$, respectively; ~25% of *C. elegans* genes are thought to be alternatively spliced; (Ramani et al., 2011). Given the established role of MEC-8 in alternative splicing, these genes are more likely to include direct targets of MEC-8. This is supported by the observation that *unc-52*, a known

target of MEC-8 (Spike et al., 2002), was among the exon-up genes identified by the array study and because a second established target of MEC-8, *mec-2*, requires MEC-8 for the removal of one of its introns (Calixto et al., 2010). Given that *mec-2* did not, however, meet all of our imposed criteria for designation as a positive outcome from the tiling array, our final gene list is likely to be missing at least some authentic MEC-8 targets.

To identify downstream targets of MEC-8 that are relevant to the synthetic phenotype of *mec-8; sym-3* and *mec-8; sym-4* mutants, we screened ~200 of the most highly misregulated genes within the dataset for enhancement of the Pin phenotype in single-mutant backgrounds (i.e., *sym-3*, *sym-4* and *mec-8*) using RNAi feeding methods. Although several gene inactivations caused low-to-moderate levels of Pin in one or more of the mutant backgrounds (data not shown), one gene, *fbn-1* (ZK783.1), led to strong enhancement of Pin in both non-RNAi-sensitized and RNAi-hypersensitive mutant backgrounds (see below). In addition, several features of *fbn-1* made it an attractive candidate as a MEC-8 target. In particular, *fbn-1* is notable in that it is one of only 12 genes within the intron-up category, and, based on fold changes, is the third most highly misregulated gene in the tiling array data set (Supplementary Files 3,4). Based on the tiling array, the region of *fbn-1* that is misregulated in *mec-8* mutants spans exons 14–19, which includes the region of *fbn-1* that is alternatively spliced (exons 14–16; Figure 4A,B). Most notably, expression of an *fbn-1* cDNA (e isoform) driven by native *fbn-1* promoter sequences partially rescued the synthetic lethality of

368 *mec-8; sym-4* mutants in two independent lines (Figure 1B). This latter finding indicates
369 that *fbn-1* is a critical target for misregulation in *mec-8; sym-4* mutants.
370
371 To confirm the tiling array results for *fbn-1*, we used PCR to amplify regions of *fbn-1*
372 from cDNA pools derived from wild-type and *mec-8* mutant embryos. Whereas primers
373 amplifying the region spanning exons 14–19 generated multiple bands of the
374 approximate expected sizes in wild type, these bands were either absent or strongly
375 reduced in *mec-8* mutants and were replaced by higher-molecular-weight, or otherwise
376 aberrant, species (Figure 4A,B). Consistent with a reduction in splicing efficiency,
377 splicing between exons 16 and 17 was largely abolished in *mec-8* mutants (Figure
378 4A,B). In contrast, splicing between exons 19 and 20 was unaffected in *mec-8* mutants,
379 consistent with both the tiling array findings and the absence of known alternative
380 splicing events between these exons (Figure 4A,B). Thus MEC-8 is required for normal
381 splicing events within the region encompassing exons 14 through 19 of *fbn-1*. The
382 observed splicing defects of *fbn-1* mRNA in *mec-8* mutants should result in a reduction
383 in the abundance of wild-type FBN-1 isoforms and reduced FBN-1 activity. In addition,
384 the presence of stop codons within introns 17 and 18 may lead to the production of
385 abnormal truncated forms of FBN-1 (Figure 4C). It is also possible that some of these
386 aberrant transcripts are targeted for degradation by RNA surveillance systems that
387 recognize abnormally long non-coding regions within mRNAs (Mango, 2001).
388
389 ***fbn-1* encodes a protein that shares some domains with vertebrate fibrillins.**

390 FBN-1 is composed of many calcium-binding and non-calcium-binding EGF-like
391 repeats, which are found in many matrix proteins and the extracellular domains of
392 transmembrane proteins (Figure 4C, Figure 4–figure supplement 2; (Davis, 1990).
393 Comparison of the predicted FBN-1 peptide sequence with mammalian sequences
394 revealed greatest sequence similarity with the family of latent TGFβ binding proteins
395 (LTBPs), which include LTBP-1, -2 and -4 and fibrillins 1–3 (Hynes, 2009; Rifkin, 2005;
396 Todorovic et al., 2005). These proteins carry out structural roles in the ECM in
397 association with elastic fibrils, mediate cell-ECM adhesion, and act as sinks or
398 reservoirs for TGFβ ligands, thereby modulating signal transduction. *C. elegans* FBN-1
399 differs from the other LTBP proteins by lacking the TGFβ binding domains and by
400 having a zona pellucida (ZP) domain. ZP domains are found in many apical ECM
401 proteins and are thought to mediate polymerization, resulting in the formation of protein
402 fibrils (Plaza et al., 2010). The presence of a furin cleavage site in FBN-1 immediately
403 after the ZP domain suggests that the extracellular domain of FBN-1 can be secreted
404 (Figure 4C; also see below). FBN-1 also contains an 834-amino-acid region (560–1393)
405 that is enriched for serine (13%) and threonine (13%) residues as well as a 179-amino-
406 acid region (1920–2098) that is enriched for serine (15%), threonine (24%) and proline
407 (13%) residues. More generally, the sequence of FBN-1, as well as its sequence
408 similarity to vertebrate LTBPs, is consistent with FBN-1 carrying out a structural function
409 in extracellular matrices affiliated with epithelial cells. We note that mis-splicing within
410 the region encompassed by exons 14–19 in *mec-8* mutants should not disrupt any
411 known protein motifs (Figure 4C). Nevertheless, this region is well conserved within

412 FBN-1 orthologs in other *Caenorhabditis* family members and is also present in more
413 distantly related parasitic species. In addition, a failure to splice out intron 17 or 18
414 would lead to a frameshift in the message and a truncated protein that lacks the ZP
415 domain and transmembrane segment.
416
417 **FBN-1 functions in a network with MEC-8, SYM-3 and SYM-4 to stabilize epidermal**
418 **architecture.**
419 Three mutant alleles of *fbn-1* were obtained for analysis including two point mutations
420 (*ns67* and *ns283*; M. Heiman and S. Shaham, unpublished data) and a deletion
421 mutation (*tm290*) generated by the *C. elegans* deletion mutant consortium (Barstead et
422 al., 2012). Both point mutations lead to non-conservative missense mutations, P116L
423 and C148A, within the first and second EGF-like repeats, respectively (Figure 4A,C,
424 Figure 4–figure supplement 2). The deletion mutation is missing 604 bp within the
425 eighth exon of *fbn-1*, which encodes a sequence that is serine and threonine rich
426 (Figure 4A,C). The *tm290* mutation should produce a protein containing the first 714
427 amino acids of FBN-1 followed by 224 novel amino acids before encountering a stop
428 codon; the *tm290* transcript may also be targeted for degradation by the non-sense
429 mediated decay pathway (Mango, 2001). Whereas the *ns67* and *ns283* alleles were
430 able to be propagated as homozygotes, *tm290* homozygotes were not easily
431 propagated and often arrested during the larval molts, consistent with a previous report
432 (Frand et al., 2005).
433

We first examined *fbn-1* alleles for the presence of the keyhole structure in embryos and the Pin phenotype in L1 larvae. Strikingly, strains containing either missense allele *ns67* or *ns283* exhibited the Pin phenotype in ~45% of their progeny, whereas *tm290* homozygotes produced by homozygous mothers carrying a rescuing *fbn-1(+)* extrachromosomal array had a lower percentage of Pin larvae (~20% within the population of array-minus progeny; Figure 5B,C; Table 1 and Supplementary File 1). Consistent with these findings, *fbn-1(RNAi)* feeding of RNAi-hypersensitive mutants gave rise to ~30% Pin larvae (Figure 5A). In addition, all three alleles of *fbn-1* led to formation of the keyhole in embryos (Figure 5C, Table 1, Supplementary File 1, data not shown). Although the penetrance of Pin in *fbn-1* single mutants was lower than *mec-8; sym-3* or *mec-8; sym-4* double mutants, the depth of the keyhole observed in some *fbn-1(tm290)* homozygous embryos exceeded that observed in *mec-8; sym-3* or *mec-8; sym-4* embryos (Figure 5C, Table 1). Thus inhibition of *fbn-1* alone can lead to a compromised embryonic sheath, making the underlying epidermis more susceptible to deformation by mechanical forces including the pulling force exerted by the pharynx. In addition, because *mec-8* homozygous animals are viable and showed a relatively low percentage of Pin larvae (Figure 1; Table 1 and Supplementary File 1), we can infer that *fbn-1* function is only partially impaired in *mec-8* mutants, consistent with our tiling array and PCR-based analyses (Figure 4B).

We next constructed double mutants between *fbn-1* and *sym-3*, *sym-4* and *mec-8* using the *ns67* and *tm290* alleles. The percentage of Pin animals in double mutants ranged

456 from 97–100%, consistent with the enhancement observed for *fbn-1(RNAi)* in RNAi-
457 hypersensitive backgrounds (Figure 5A–C, Supplementary File 1). In addition, the
458 average depth of the keyhole in these embryos was typically greater than that observed
459 for *mec-8; sym-3* or *mec-8; sym-4* mutants as well as for *fbn-1* single mutants (Table 1).
460 Notably, certain double-mutant combinations displayed phenotypes that had not been
461 previously observed in *mec-8; sym-3* or *mec-8; sym-4* mutants or in *fbn-1* single
462 mutants. In the case of *fbn-1(tm290); sym-3* and *fbn-1(tm290); sym-4* mutants, large
463 lumps or protuberances on the head region were observed in L1 larvae (Figure 5C),
464 which are reminiscent of certain phenotypes observed in integrin pathway mutants
465 (Baum and Garriga, 1997; Tucker and Han, 2008).
466
467 Interestingly, *mec-8; fbn-1(tm290)* mutants arrested uniformly as embryos and failed to
468 complete embryonic elongation (Figure 5C). These embryos displayed a deep keyhole
469 by the 1.5-fold stage (Table 1 and Supplementary File 1), and by the ~2-fold stage 92%
470 (n=73) exhibited prominent epidermal ingressions and furrows, which were often
471 regularly spaced (Figure 5C). Notably, this phenotype was previously observed after
472 digestion of the embryonic sheath with trypsin (Priess and Hirsh, 1986), suggesting that
473 FBN-1 carries out mechanostructural functions throughout the embryonic sheath
474 including a role in stabilizing the epidermis during circumferential constriction.
475 Consistent with this interpretation, inhibition of epidermal actomyosin contraction using
476 *let-502(RNAi)* reduced the frequency of *mec-8; fbn-1(tm290)* embryos that contained
477 deep furrows to 17% (n=52; Figure 5C). We note that in addition to surface furrows and

478 blobs, some *mec-8; fbn-1(tm290)* embryos also showed cell detachment phenotypes
479 (Figure 5C), suggesting that MEC-8 and FBN-1 promote epidermal integrity. Because
480 *tm290* is likely to constitute a null mutation in *fbn-1*, we interpret the severe phenotype
481 of *mec-8; fbn-1(tm290)* mutants to indicate that MEC-8 regulates additional proteins that
482 act redundantly with FBN-1 together to promote normal epidermal structure and
483 morphogenesis.
484
485 **Activity of *fbn-1* is required in the epidermis.**
486 On the basis of the above findings, we hypothesized that FBN-1 is a component of the
487 embryonic sheath, a specialized ECM secreted from the apical surface of epidermal
488 cells that promotes structural stability and resistance to biomechanical forces (Priess
489 and Hirsh, 1986). A requirement for *fbn-1* in the epidermis was first tested by treating
490 wild-type and NR222 strains with *fbn-1(RNAi)* using standard feeding methods.
491 Whereas wild-type strains can undergo “systemic” RNAi (throughout the majority of
492 tissues), NR222 is engineered to undergo RNAi in the epidermis only (Qadota et al.,
493 2007) Figure 5A, Figure 6A, Supplementary File 1). Although RNAi of *fbn-1* failed to
494 produce any visible phenotype in these strains, enhancement of the Pin phenotype was
495 observed in an NR222 derivative that carried a *mec-8* mutation ($P < 0.01$), implicating
496 the epidermis as critical for *fbn-1* activity (Figure 6A and Supplementary File 1).
497
498 Genetic mosaics (Yochem and Herman, 2005) were also examined for the focus of *fbn-*
499 *1* activity in the prevention of the Pin phenotype. This non-biased approach used an *fbn-*

500 *1(tm290); sym-4(mn619)* strain carrying a rescuing *fbn-1(+)* extra-chromosomal array,
501 *fdEx249*, that also expresses a fluorescent reporter, *sur-5::GFP*, to assess mitotic
502 inheritance of the array (Yochem et al., 1998). This strain segregated array-minus Pin
503 progeny, array-plus viable progeny and array-plus viable progeny that were mosaic for
504 inheritance of the array; array-minus non-Pin *fbn-1(tm290); sym-4(mn619)* animals were
505 not observed. Based on numerous mosaics, *fbn-1* activity is focused in hyp6, the
506 anterior portion of the hyp7 syncytium, or both hyp6 and hyp7. An exact determination
507 of inheritance was not possible because both the hyp6 and hyp7 syncytia initiate
508 formation through cell fusion near the time the keyhole (Pin) becomes apparent and the
509 hyp6 syncytium fuses with the hyp7 syncytium late in the L2 stage (Yochem et al.,
510 1998). Nevertheless, two mosaics proved particularly informative in that hyp7 was the
511 only positive tissue. Moreover, SUR-5::GFP was expressed in an anterior-to-posterior
512 gradient in both mosaics, suggesting establishment of the positive clone within the hyp7
513 syncytium by one or more hyp6 cells, which are anterior, or possibly one or more
514 anterior hyp7 cells. Additional mosaics were consistent with a requirement for *fbn-1(+)*
515 in anterior epidermal cells. For example, in 16 mosaics, only AB, one of the daughters
516 of the zygote, had established a positive clone (Figure 6B). In contrast, there were no
517 reciprocal mosaics in which P1, but not AB, had established a positive clone. Although
518 12 of the hyp7 cells of the embryo descend from P_1, these cells are not located as far
519 anterior in the embryo as are certain hyp7 (or hyp6) cells that descend from AB (Sulston
520 et al., 1983). In addition to these 16 AB(+)P_1(–) mosaics, there were 25 mosaics in
521 which positive clones had been established within the AB sublineage only. In every

522 case, these clones contributed descendants to hyp6 or to the anterior part of hyp7
523 (Figure 6B).
524
525 Although the genetic mosaics are consistent with the epidermal-specific RNAi described
526 above, the mosaics cannot eliminate other anterior epidermal cells as important for
527 expression of *fbn-1*. For example, although hyp4 cells, which are closer to the sensory
528 depression than hyp6 or hyp7 cells, were not specifically implicated in the analysis, they
529 could still contribute significant FBN-1 for proper function of the sheath in wild-type
530 embryos. For example, a contribution by hyp4 could be obviated in mosaics by over-
531 expression of *fbn-1* in hyp6 or anterior hyp7 cells, particularly if it is diffusible following
532 secretion from the apical surface of these cells. In fact, a requirement for *fbn-1* in the
533 sheath surrounding hyp4 is consistent with the observed deformation of hyp4 cells in
534 *fbn-1* mutants (Figure 6C). Neither sheath nor socket cells associated with the sensory
535 depression were implicated in the mosaic analysis, underscoring the requirement for
536 *fbn-1* expression in the epidermis for the prevention of Pin. Also of note, the molting
537 defect associated with *fbn-1(tm290)* was rescued in all of the non-Pin mosaics. Thus,
538 the epidermis appears to be the sole focus for both major aspects of the *fbn-1*
539 phenotype.
540
541 **FBN-1 is expressed in embryonic epidermal cells and secreted to the apical**
542 **surface.**

To more directly assess *fbn-1* expression in live embryos, we used strains that contained one of two *fbn-1* fluorescent reporters. $P_{fbn\text{-}1}$::GFP-PEST is expressed under the control of the native *fbn-1* promoter and contains PEST sequences, which reduce the half-life of GFP (Frand et al., 2005). $P_{fbn\text{-}1}$::GFP-PEST expression was first detected in epidermal cells at the onset of embryonic morphogenesis, and expression continued throughout embryogenesis (Figure 6D). The mini-*fbn-1*::mCherry reporter includes both an N-terminal region (aa 1–48) that contains a predicted signal peptide (aa 1–26) and a portion of the C terminus (aa 2418–2781) that includes the ZP domain (aa 2438–2674), the furin cleavage site (aa 2676–2679) and the predicted transmembrane segment (aa 2745–2767). mini-*fbn-1*::mCherry localized to the apical surface of epidermal cells coincident with the location of the embryonic sheath (Figure 6D). Expression was first detected during early stages of morphogenesis and increased in intensity through the 1.5-fold stage, consistent with the timing of embryonic sheath formation (Figure 6D; (Priess and Hirsh, 1986). mini-*fbn-1*::mCherry was also detected during late stages of embryogenesis and in larvae (to be described elsewhere). Notably, mini-*fbn-1*::mCherry was detected in the extra-embryonic space of early morphogenetic embryos, consistent with apical secretion of the fusion proteins (Figure 6D). The expression of FBN-1 in epidermal cells and its secretion to the apical surface is consistent with the model that FBN-1 functions as a structural component of the embryonic sheath where it prevents mechanical deformation of the epidermis.

The embryonic sheath prevents epidermal deformation by multiple forces. Priess and Hirsch (1986) used laser permeabilization of the eggshell followed by trypsin treatment to induce digestion of the embryonic sheath. Although they reported striking indentations or furrows at the surface of ~2-fold-stage trypsin-treated embryos, similar to what we observed for *mec-8; fbn-1(tm290)* mutants (Figure 5C), defects of the sensory depression were not described. We therefore carried out a similar experiment in which we used chitinase to partially or completely digest the eggshell followed by trypsin treatment. Most notably, we detected keyholes in ~1.5- to 3.0-fold-stage embryos, as well as mild ingressions at the surface of some embryos (Figure 7A). We note that the surface ingressions we observed were less dramatic than those reported in the previous study, which may be due in part to the different methods used to permeabilize the eggshell. Epidermal ingressions induced by trypsin treatment were also less severe than those observed for *mec-8; fbn-1(tm290)* mutants (Figure 5C), suggesting that the sheath was more severely compromised in these double mutants. Of interest, keyholes were seen in some embryos that lacked other obvious morphological defects (data not shown), suggesting that the region of the pharyngeal attachment is particularly sensitive to deformation after partial degradation of the sheath. These findings were also consistent with the lack of gross morphological defects seen in *fbn-1* single mutant embryos as well as *mec-8; sym-3* or *mec-8; sym-4* double mutants, which nevertheless had a prominent keyhole and Pin phenotype. We note that the pharyngeal cuticle contains the polysaccharide chitin and thus treatment with chitinase could be expected to preferentially degrade the pharyngeal cuticle as well

as the eggshell (Zhang et al., 2005). Nevertheless, the penetrance of Pin was ~10-fold higher in embryos treated with both trypsin and chitinase relative to chitinase alone (data not shown), consistent with a role for sheath proteins in preventing mechanical deformation of cells surrounding the sensory depression.

DISCUSSION

Force is essential for shaping the embryo and its internal organs (Davidson, 2011; Davidson, 2012; Heisenberg and Bellaiche, 2013; Keller et al., 2003; Keller et al., 2008), and spatiotemporal application of tightly controlled forces ensures normal morphogenesis. Proper development also requires that cells and tissues that experience forces respond in a consistent and context-appropriate manner. Either too much or too little resistance on the part of targeted tissues can lead to morphogenetic abnormalities and birth defects (Epstein et al., 2004; Moore et al., 2013).

Our studies have implicated FBN-1, along with MEC-8, SYM-3 and SYM-4, in promoting correct epidermal morphology and resistance of the *C. elegans* epidermis to two biomechanical forces. One force is generated by the circumferential constriction of epidermal actomyosin rings and was identified nearly 20 years ago as the major driver of embryonic elongation (Priess and Hirsh, 1986). We have described here a second force in which the elongating pharynx exerts an inward pull on the anterior epidermis throughout much of embryonic development. Although the potential for a pulling force was suggested by a previous study describing early steps of pharyngeal morphogenesis (Portereiko and Mango, 2001), this force was not characterized in any detail. Our studies suggest that this force may result from an intrinsic mechanical resistance of the embryonic pharynx to stretching. Moreover, the epidermal constricting force and pharyngeal stretching force are mechanistically linked because extension of the pharynx requires elongation of the epidermis. We also note that whereas inhibition of *fbn-1* alone

led to decreased resistance to the pharyngeal pulling force, deformation of the lateral epidermis by the circumferential constricting force required the simultaneous loss of *fbn-1* and *mec-8*, indicating that additional targets of MEC-8 likely contribute to epidermal stability.

Our studies indicate that FBN-1, a protein that is related to fibrillin, is critical for biomechanical force resistance by the epidermis during development. FBN-1 was broadly expressed in the embryonic epidermis and was secreted to the apical surface as a putative component of the embryonic sheath. In Pin embryos that lacked wild-type *fbn-1* activity, progenitor cells of the hyp4 epidermal syncytium became hyperextended. Although hyp4 cells were not directly implicated as the focus for *fbn-1* expression by the mosaic analysis, secreted ECM proteins can rescue defects at a distance or when expressed from cell types that are not normally the source of the protein product (Heiman and Shaham, 2009). This is particularly true if proteins are overexpressed, as is often the case for mosaic analysis. The lack of identified mosaic animals in which hyp4 was the only positive epidermal clone may be due to their low frequency of occurrence or because expression of *fbn-1* in hyp4 is not essential for rescue of Pin if other neighboring cells secrete high levels of FBN-1. Alternatively, expression of FBN-1 in hyp6/7 progenitors could possibly alter the biophysical properties of the sheath and the tension on hyp4 cells. More generally, our findings implicate *fbn-1* expression in the anterior epidermis as critical for suppression of the Pin phenotype. In addition, analysis of *mec-8; fbn-1* double mutants indicated a role for FBN-1 throughout the embryonic

636 sheath in resisting or properly distributing forces that arise during circumferential
637 constriction of the epidermis.
638
639 We failed to detect morphological defects at the attachment site of the intestine to the
640 rectum in any of the mutant backgrounds examined. Although it is possible that
641 stretching of the intestine during embryonic elongation may also lead to forces that act
642 on the posterior epidermis of the worm, such forces may be lower in magnitude than
643 those experienced at the anterior, possibly because of structural differences between
644 the pharynx and intestine.
645
646 A number of human diseases that affect ECM components can lead to altered
647 mechanical properties of the skin and other connective tissues, which may parallel
648 defects observed in *C. elegans fbn-1* mutants. (Judd, 1984; Milewicz et al., 2000). This
649 includes mutations in human fibrillin 1, which is mutated in Marfan syndrome. (Dietz et
650 al., 2005; Ramirez and Dietz, 2009; Ramirez and Sakai, 2010). Although our findings
651 suggest that FBN-1 and human fibrillins may carry out some related functions in the
652 ECM, structural differences between FBN-1 and vertebrate fibrillins suggest significant
653 functional divergence (Piha-Gossack et al., 2012). For example, FBN-1 lacks conserved
654 TGFβ binding sites found in human fibrillins and contains a ZP domain not found in
655 LTBP family proteins. Thus, whereas mammalian fibrillins and other members of the
656 LTBP family of proteins have secondary roles in modulating signal transduction, their
657 closest counterparts in nematodes may be limited to structural functions only. In

addition, mammalian fibrillins interact with elastins (Baldwin et al., 2013), which are not present in *C. elegans*. A phylogenetic analysis suggested that fibrillins may have been lost or severely disrupted in the nematode lineage as well as in *Drosophila*, although apparent fibrillin orthologs are present in several insect species including ants and honeybees (Piha-Gossack et al., 2012).

Our findings in *C. elegans* suggest that FBN-1 is required in the embryonic sheath to ensure the appropriate level of resistance to mechanical deformation by inward-pulling forces (Figure 7B), a function originally proposed for the sheath by Priess and Hirsch (1986). This could be because FBN-1 directly affects the resilience of the embryonic sheath, thereby influencing the response of attached epidermal cells to mechanical forces. Alternatively, FBN-1 may be required for the stable attachment of epidermal cells to the sheath or the efficient transmission and distribution of forces throughout the sheath. For example, FBN-1 in the sheath could interact with other transmembrane proteins expressed on the apical surface of the epidermis, consistent with the presence of putative integrin (Arg/Gly/Asp; RGD) binding sites in FBN-1 (Figure 4–figure supplement 2). In this latter scenario, inward-pulling forces may physically detach epidermal cells from the overlying sheath in mutants with compromised *fbn-1* function, leading to excessive or atypical deformation of the unattached epidermis. In addition, it is also possible that FBN-1 could promote attachment of the epidermis to the sheath through its transmembrane domain, although cleavage of FBN-1 by furin proteases, a

679 post-translational processing event conserved in human fibrillins (Ashworth et al., 1999;
680 Lonnqvist et al., 1998), make this mechanism less likely.
681
682 More generally, our results suggest that mechanical properties of the aECM strongly
683 affect epidermal cell architecture and embryonic morphogenesis. Although originally
684 thought to function exclusively as a protective barrier to the environment, the aECM has
685 recently been recognized to play key roles in epithelial morphogenesis, tube formation
686 and cell junction stability (Brown, 2011; Hynes, 2009). In *C. elegans*, several aECM
687 proteins containing extracellular leucine-rich only (eLLRon) repeats are required to
688 maintain the integrity of epithelial junctions within the lumen of the excretory system
689 (Mancuso et al., 2012) and to promote dendrite branching (Liu and Shen, 2012).
690 Correspondingly, the *Drosophila* eLLRon protein dALS/convoluted is required to
691 organize the tracheal lumen matrix, and mutations in *dALS* lead to tracheal tube
692 morphogenetic defects (Beitel and Krasnow, 2000; Swanson et al., 2009). A second
693 class of aECM protein, those containing a ZP domain, have been implicated in
694 tubulogenesis and epithelial morphogenesis in *Drosophila* (Denholm and Skaer, 2003;
695 Dong et al., 2014; Jazwinska et al., 2003; Plaza et al., 2010; Roch et al., 2003). The
696 *Drosophila* ZP-domain protein DPY has been proposed to organize cuticle architecture
697 and to anchor the cuticle to the epidermis. Based on its size, structural motifs and
698 mutant phenotypes, DPY has been proposed to distribute mechanical tension within the
699 cuticle, thereby stabilizing the attachment of the epidermis to the cuticle (Wilkin et al.,
700 2000). Notably, *dpy* is the closest *Drosophila* relative to *C. elegans fbn-1*, and their

related mutant phenotypes suggest strong functional conservation. In *C. elegans*, DYF-7, a ZP-domain protein, and DEX-1, which contains a zonadhesin domain, are required to anchor dendrite endings at the nose while the neuronal cell bodies migrate away, stretching the dendrites behind them as they migrate (Heiman and Shaham, 2009). These neurons may experience mechanical tension during the process of retrograde dendritic extension, and mutations in *dex-1* or *dyf-7* lead to morphogenetic defects in these neurons and associated glia. In addition to eLLRon and ZP-domain proteins, several other classes of aECM proteins have been implicated in epithelial morphogenesis in *C. elegans*, *Drosophila* and other species (Labouesse, 2012; Lane et al., 1993; Luschnig and Uv, 2014; McLachlan and Heiman, 2013; Moussian et al., 2007; Syed et al., 2012; von Kalm et al., 1995; Willenborg and Prekeris, 2011). Because our tension sensor records molecular tension only within UNC-70/β-spectrin, it remains unclear how the observed intracellular tension is related to tension in the aECM. Further studies of the mechanical resistance of the embryonic sheath and the forces transmitted through cell-adhesion and matrix-anchoring molecules are needed to elucidate this important aspect of morphogenesis.

Although our studies demonstrate that FBN-1 is an important downstream target of MEC-8 in promoting force resistance by the epidermis, it is clearly not the only target of MEC-8 that carries out structural or biomechanical functions. Cytoskeletal and ECM proteins implicated by the *mec-8* tiling array studies include AJM-1, a component of epithelial adherens junctions (Koppen et al., 2001); LET-805, a fibronectin repeat

723 protein (Hresko et al., 1999); UNC-52/perlecan, a component of basement membranes
724 (Rogalski et al., 1993); VAB-10/plakin a cytoskeletal crosslinker (Bosher et al., 2003)
725 and UNC-70/β-spectrin (Hammarlund et al., 2000). Based on our genetic data,
726 misregulation of *fbn-1* may largely account for the role of *mec-8* in the context of its
727 synthetic phenotype with *sym-3* or *sym-4*, although one or more additional MEC-8
728 targets may contribute to the anterior epidermal defects of *mec-8; sym-3* or *mec-8; sym-*
729 *4* double mutants. Furthermore, the synthetic embryonic lethality observed in *mec-8;*
730 *fbn-1(tm290)* double mutants (Figure 5C) indicates that MEC-8 regulates the splicing of
731 one or more genes that function redundantly with FBN-1.
732
733 Similar to *C. elegans mec-8*, mutations in the *Drosophila mec-8* ortholog, c*oach potato*
734 *(cpo)*, lead to neuronal and behavioral defects (Bellen et al., 1992a; Bellen et al., 1992b;
735 Glasscock and Tanouye, 2005; Perkins et al., 1986), although the splicing targets of
736 Cpo are unknown. In addition, *cpo* is implicated in diapause regulation and climatic
737 adaptation through an unknown mechanism (Schmidt et al., 2008). RBPMS and
738 RBPMS2, the human orthologs of MEC-8, are broadly expressed but very little is known
739 about their targets or biological functions (Shimamoto et al., 1996). Interestingly, human
740 *FBN1* and *FBN3* are alternatively spliced and distinct *FBN1* isoforms are expressed in a
741 tissue and developmental-specific manner (Biery et al., 1999; Burchett et al., 2011;
742 Corson et al., 1993; Corson et al., 2004). Furthermore, alternative splicing of *FBN1* has
743 been suggested to modulate the severity of Marfan syndrome (Burchett et al., 2011).
744 Although it is tempting to speculate that RBPMS could be a candidate regulator of

745 human fibrillins, it must be noted that the region of *fbn-1* that is regulated by MEC-8
746 (e14–e19) is not conserved outside of nematodes nor is the RNA recognition sequence
747 for MEC-8/Cpo/RBPMS currently known.
748
749 How SYM-3 and SYM-4 promote epidermal stability or ECM maintenance is at present
750 unresolved. SYM-4 is a predicted β-propeller protein with seven WD-repeats,
751 suggesting a role in coordinating protein interactions. Two independent groups identified
752 mammalian SYM-4, WDR44, as a binding partner and candidate effector of the Rab11
753 GTPase (Mammoto et al., 1999; Zeng et al., 1999). WDR44 associates specifically with
754 the activated GTP-bound form of Rab11 and partially co-localizes with Rab11
755 (Mammoto et al., 1999; Zeng et al., 1999). Rab11 has been studied in multiple contexts
756 and is primarily associated with the regulation of trafficking to and from the endocytic
757 recycling compartment (Grant and Donaldson, 2009; Horgan et al., 2010; Kelly et al.,
758 2012; Ren et al., 1998; Urbe et al., 1993) but also functions in exocytosis and in
759 conjunction with the exocyst complex (Chen et al., 1998; Sato et al., 2008; Satoh et al.,
760 2005; Takahashi et al., 2012; Ward et al., 2005; Welz et al., 2014) and in Golgi-
761 endosome transport (Ullrich et al., 1996; Wilcke et al., 2000). In *C. elegans*, RAB-11
762 regulates endosomal recycling during mitosis (Ai et al., 2009; Blethrow et al., 2004),
763 cytokinesis (Bembenek et al., 2010) and meiosis (Cheng et al., 2008) and, most
764 notably, promotes secretion and ECM formation in embryos (Sakagami et al., 2008;
765 Wehman et al., 2011). Based on a high-throughput screen, the *Drosophila* SYM-4
766 ortholog, CG34133, physically interacts with Amph/Amphiphysin (Guruharsha et al.,

767 2011), a BAR-domain protein that promotes endocytosis through membrane bending
768 and vesicle fission (Campelo and Malhotra, 2012; Cowling et al., 2012; Peter et al.,
769 2004), suggesting that SYM-4 may interact directly with components of the vesicular
770 trafficking machinery.
771
772 SYM-3 contains an N-terminal C2 domain (NT-C2/EEIG1/EHBP1), which suggests an
773 association with the cytoplasmic surface of cell membranes (Zhang and Aravind, 2010).
774 Intriguingly, the physical interaction between WDR44 and Rab11 was previously
775 proposed to require an unidentified membrane-associated factor (Zeng et al., 1999).
776 The only other *C. elegans* NT-C2 protein, EHBP-1, is a co-partner of RAB-10 in
777 endocytic recycling (Shi et al., 2010) and an NT-C2 domain is present in the mammalian
778 Rab11 interactor, Rab11-FIP2 (Hales et al., 2002; Welz et al., 2014). The *Drosophila*
779 SYM-3 ortholog, CG8671, is required for efficient dsRNA uptake, a process that
780 requires receptor-mediated endocytosis (Saleh et al., 2006). Correspondingly, *sym-3*
781 inhibition may lead to a modest reduction in the sensitivity of *C. elegans* to RNAi feeding
782 (Saleh et al., 2006). Thus, although their specific molecular functions are largely
783 uncharacterized, available evidence points to a role for both SYM-3 and SYM-4 in
784 vesicular trafficking and endocytosis and/or endocytic recycling.
785
786 We propose that SYM-3 and SYM-4 may co-regulate the cell-surface trafficking of one
787 or more proteins that regulate epidermal stability. Loss of *sym-3* or *sym-4* activity could
788 potentially result in the mislocalization of one or more integral membrane proteins or

789 ECM components required for normal resistance to mechanical stress.
790 Correspondingly, the combined loss of both *mec-8* and either *sym-3* or *sym-4* activity
791 most likely to a synergistic effect on the epidermis and the observed synthetic
792 phenotype. SYM-3 and SYM-4 may regulate the secretion of aECM proteins, such as
793 FBN-1, or may control the trafficking of integral membrane proteins required for the
794 adhesion of epidermal cells to the aECM or possibly other cell types. We note that the
795 lack of any molting defect in *mec-8; sym-3* and *mec-8; sym-4* mutants, a phenotype
796 observed following strong loss of function of *fbn-1*, is perhaps most consistent with
797 SYM-3 and SYM-4 acting on a target distinct from FBN-1. In any case, the roles of
798 MEC-8, SYM-3 and SYM-4 in morphogenesis are revealed only under genetic
799 conditions in which overlapping or redundant functions are inhibited. Further studies to
800 fully understand the basis for morphogenesis and the role of the aECM in development
801 are also likely to require approaches that address and overcome limitations imposed by
802 genetic redundancy.
803

Materials and methods

Strains and maintenance.

All strains were cultured on nematode growth medium (NGM) supplemented with *E. coli* OP50 as a food source according to standard protocols (Stiernagle, 2006) and were maintained at 20ºC except for strains containing the *sqt-3(e2117)* allele. Strains used in this study included N2, SP2231 [*sym-3(mn618) X*], SP2232 [*sym-4(mn619) X*], WY893 [*mec-8(u74) I; sym-3(mn618) X; mnEx169 (sym-3(+);sur-5::GFP)*], WY969 [*mec-8(u74) I; sym-4(mn619) X; fdEx226 (sym-4(+); sur-5:GFP; P_{hsp-16}::peel-1*], SP1750 [*mec-8(u74) I; mnEx2 (mec-8(+); pRF4rol-6(su1006d))*], WY870 [*mec-8(u74) I; pha-1(e2123ts) III; sym-3(mn618) X; mnEx169*], WY873 [*mec-8(u74) I; pha-1(tm3671) III; sym-3(mn618) X; mnEx169; fdEx201 (PBX(pha-1(+); sur-5::RFP)*], WY965 [*lin-35(n745) I; sym-3(mn618) X*], WY964 [*lin-35(n745) I; sym-4(mn619) X*], GE24 [*pha-1(e2123ts) III*], WY849 [*pha-1(tm3671) III; fdEx183* (pBX; *sur-5::GFP*)], CHB11 [*fbn-1(ns67) III; oyIs44 [odr-1::RFP] V*], CHB31 [*fbn-1(ns283) unc-32(e189) III; kyIs136 (str-2pro::GFP) X*], WY1034 [*fbn-1(tm290) III; fdEx249 (sur-5::GFP; fbn-1(+)-fosmid wrm0635cH08)*], WY1048 [*fbn-1(ns67) III; oyIs44 V; sym-3(mn618) X; mnEx169*], WY1049 [*fbn-1(ns67) III; oyIs44 V; sym-4(mn619); fdEx225 (sym-4(+); sur-5::GFP*], WY1056 [*mec-8(u74) I; fbn-1(ns67) III; oyIs44; fdEx249*], WY1057 [*fbn-1(tm290) III; sym-3(mn618) X; fdEx249*], WY1058 [*fbn-1(tm290) III; oyIs44 V; sym-3(mn618) X; fdEx249*], WY1068 [*mec-8(u74) I; fbn-1(tm290) III; fdEx249*], CB4121 [*sqt-3(e2117) V*], *mec-8(u74) I; sqt-3(e2117) V*], ARF256 [*aaaEx32 (Pfbn-1::gfp-pest + Pttx-3::GFP)*], ARF262 [*aaaEx33 (fbn-1Δ49-2418::mCherry+ P_{myo-2}::GFP)*], WY1082 [*fbn-1(ns67); aaaEx32*], GN517 [*pgEx116 (unc-*

826 *70-TSmod; myo3::mCherry)*], GN519 [*pgEx131* (*unc-70*(5aa) p*unc-122*::RFP)], GN518
827 [*pgEx126* (*unc-70*(TRAF); p*unc-122*::RFP)], GN600 [*pgIs22* (*unc-70(N-TSMod)), oxIs95*
828 *(myo2::gfp; pdi-2::unc-70)V*], WY1047 [*pha-1(tm3671) III; fdEx182; pgEx116*], GN486
829 [*unc-70(s1502)V; oxIs95 IV; pgEx126*], GN491 [*unc-70(s1502)V; oxIs95IV; pgEx131*],
830 GN601 [*unc-70(s1502) V; oxIs95 IV; pgIs22*], NR222 [*rde-1(ne219) V; kzIs9*
831 *(pKK1260(lin-26p::nls::GFP); pKK1253(lin-26p::rde-1); pRF6(rol-6(su1006))*], WY1033
832 [*mec-8(u74) X; rde-1(ne219) V; kzIs9*].
833
834 **Tension sensor studies.**
835 Generation of transgenic animals: A detailed description of the molecular cloning of the
836 *unc-70* cDNA and TSMod derivatives is found in Krieg et al, 2014. Transgenesis was
837 performed by microinjection following standard procedures. We also assayed the ability
838 of the UNC-70(TSMod) as well as the low FRET, high FRET and no-force transgenes to
839 rescue the locomotion defect of *unc-70(s1502)* mutants. To do so, we placed transgenic
840 animals onto fresh agar plates and recorded short movies (<1 min) and compared the
841 movement (curvature matrices) of transgenic animals to the parental *unc-*
842 *70(s1502);oxIs95* mutants (Hammarlund et al., 2007) and to wild-type animals. All
843 constructs [UNC-70(TSMod) *pgEx116*, UNC-70(TRAF) *pgEx126*, UNC-70(5aa)
844 *pgEx131* and UNC-70(N-TSMod) *pgIs22*] were capable of restoring locomotion to
845 paralyzed *unc-70(s1502);oxIs95* adults (data not shown).
846
847 Imaging acquisition: Förster resonance energy transfer (FRET) images were acquired

and processed as described in detail in Krieg et al, 2014. In short, three images for each focal plane and time point were taken at 512×512 pixels and with a 400-Hz acquisition rate using a Leica SP5 confocal microscope. The three images were: 1) donor emission after direct donor excitation, 2) acceptor emission after direct excitation of the acceptor and 3) acceptor emission after excitation of the donor, representing the raw uncorrected image. In total, a *z*-stack of the whole embryo was taken, and frames encompassing the buccal cavity were analyzed (3-5 frames on average). Before processing, all images were binned (downsampled and averaged) once to increase the signal-to-noise ratio and imported into IgorPro (WaveMetrics, Oregon) for further processing. A pre-calibration of the microscope using a solution of 0.01% fluorescein showed that detector gains are linear within the laser power range used for these studies.

Image processing: The raw FRET image was background subtracted and corrected for bleed through using pre-determined values for each bleed-through factor (Krieg et al., 2014) according to $cF\,(i,j\,) = I_F\,(i,j\,) - \delta \cdot I_D\,(i,j\,) - \alpha \cdot I_A\,(i,j\,)$ in which α and δ are the measured bleedthrough factors for the acceptor and the donor channel, respectively (Krieg et al., 2014), and i,j are the pixel coordinates. The final FRET index image was calculated according to $F = \frac{cF \cdot Q_D \cdot {\varphi_D}/{\varphi_A}}{qD + (cF \cdot Q_D \cdot {\varphi_D}/{\varphi_A})}$ on a pixel-by-pixel basis (Chen and Periasamy, 2006; Krieg et al., 2014) in which *cF* is the bleedthrough corrected FRET channel intensity, Q_d is the quantum yield of the donor fluorophore and was empirically determined (Day et al., 2008), and *qD* is the quenched donor intensity. The ratio ${\varphi_D}/{\varphi_A}$ is the collection efficiency and has been determined empirically (Krieg et al.,

2014). A [3×3] median filter was applied to remove high-frequency noise in the FRET map.

Final quantification and ROI selection: The FRET index image was quantified by manually selecting a box (region of interest (ROI), Figure 3) over the putative pharynx attachment site to the epidermis (sensory depression region, SDR). More specifically, The SDR ROIs were identified as the area of the highest intensity and curvature around the sensory depression of the epidermis. In *pha-1* mutants, the sensory depression was identified as the region directly anterior to the (non-attached) primordial pharynx. A second ROI (non-SDR) was then chosen that encompassed the remainder of the embryo (excluding the SDR) and, therefore, was larger than the ROI of the SDR. The rational was to create an `internal' reference value, to which the SDR can be compared, which is independent of differences in sensor expression level, variations in bleedthrough, bleaching, and downstream image processing procedures, as every pixel in an image has the exact same history. Because the precise size of the ROIs varied between embryos, the number of pixels within individual SDR ROIs and non-SDR ROIs was also variable. A pairwise comparison between SDR and non-SDRs within individual embryos was carried out to assess variations of FRET values independent of different expression levels among different embryos.

To evaluate the quality of our measurements and robustness against uncontrolled changes in intensity due to stochastic shot noise, we calculated the uncertainty of the

FRET values derived from UNC-70(N-TSMod) embryos (since they do not show differences in FRET due to tension) in each pixel by error propagation (Berney and Danuser, 2003). Pixels with low intensity show high uncertainty. To minimize the impact of this source of error, we limited our analysis to those pixels within each ROI whose intensity exceeded a threshold. This strategy also selects domains in which the sensor is concentrated (i.e. cell cortices) and excludes those that lack sensor molecules (i.e. cytoplasm). No significant correlation of the FRET index with the expression level (acceptor counts) was observed, indicating that intermolecular FRET had a negligible contribution to the final FRET index image (data not shown; (King et al., 2014).

Statistical evaluation: FRET index values from different planes encompassing the buccal cavity within a given embryo were pooled, and the average was treated as an experimental value. Statistical significance was assessed using a two-tailed t-test to compare intra-embryonic ROIs and ROIs between embryos. Data were normally distributed as determined using the Jarque-Bera test for normality and exhibited equal variance as judged by Levene's test. Comparison of FRET values was carried out using a Student's T test and paired T-tests (where applicable; Supplementary File 2) and the Mann-Whitney U-test (data not shown).

Tiling array studies.

Wild-type *C. elegans* (N2) and *mec-8*(*u314*) animals were grown at 20°C on high peptone plates (Zhang et al., 2002) until gravid. Embryos were extracted with a solution

911 that contained 1 M NaOH and 30% bleach, in water. Total RNA from embryos was
912 extracted using TriReagent (Sigma) and cleaned using RNeasy columns (QIAGEN)
913 according to the manufacturer's protocol. Purified RNA was then treated with 10 U
914 DNase I (Roche) for 30 min in 100 μl 1× One-Phor-All buffer (Amersham). The RNA
915 was then re-purified with RNeasy columns (QIAGEN) and 1 μl random hexamers (3
916 μg/μl) was added to 15 μg purified total RNA together with reverse transcriptase. The
917 (ds)cDNA was then purified using QIAGEN PCT purification columns, and 17 μg of
918 (ds)cDNA was digested and labeled using standard Affymetrix methods The
919 hybridization cocktail was injected into an Affymetrix GeneChip *C. elegans* Tiling 1.0R
920 Array. Hybridized microarrays were washed and scanned according to chapter 5 of the
921 GeneChip Whole Transcript (WT) Double Stranded Target Assay Manual
922 (https://www.affymetrix.com/support/downloads/manuals/wt_dble_strand_target_assay_
923 manual.pdf). For reverse transcriptase PCR studies of select MEC-8 targets identified
924 by the tiling array (Figure 4 – figure supplement 1), total RNA used for the tilling array
925 experiments was reverse transcribed using oligo-dT primers and amplified using
926 specific primers for each gene region (Supplementary File 5) for 30 cycles.
927
928 **PCR analysis of *fbn-1*.**
929 Total RNA from N2 and *mec-8(u74)* embryos was isolated using Trizol and purified on
930 RNeasy minicolumns (QIAGEN). cDNA was prepared from 1 μg RNA using a
931 SuperScript II first-strand synthesis system (Invitrogen) and analyzed by PCR (30 and
932 35 cycles) using the following primers: 5'-CAACAGAGTCATCCGAAGCT-3' and 5'-

TGCAGTTGTGGTGGTGGTAGGT-3' (which anneal to exon 16 and exon 17 of *fbn-1*, respectively), 5'- GACAGGAAAAACCAACTACTAAA-3' and 5'-TGTGACTGTGGAGCAAAGAGATG-3' (which anneal to exon 14 and exon 19 of *fbn-1*, respectively) and 5'-TGTCTTCCAGGATTTACTGGAG-3' and 5'-TACATACTGCGTTCGGGTG-3' (which anneal to exon 19 and exon 20 of *fbn-1*, respectively).

RNAi.

RNAi-feeding was done with strains from the Geneservice Library, using the standard feeding protocol (Ahringer, 2005). Control RNAi-feeding assays were carried out using a bacterial strain carrying the RNAi vector pDF129.36, which produces an ~200-bp dsRNA that is not homologous to any *C. elegans* gene (Timmons et al., 2001). RNAi hypersensitive mutations used included *lin-35(n745)* (Lehner et al., 2006; Wang et al., 2005) and *rrf-3(pk1426)* (Simmer et al., 2002). For *let-502(RNAi)* of *mec-8; fbn-1* mutants, dsRNA targeting *let-502* exon 4 was injected into P0s at a concentration of ~500 ng/µl and F1s laid between 24–48 hours post injection were scored.

Mosaic analysis.

Mosaic analysis was carried out using strains WY1059, *fbn-1(tm290); sym-4(mn619); fdEx249[fbn-1(+); sur-5::GFP]*, and WY1068, *mec-8(u74)*; *fbn-1(tm290); fdEx249*, following established protocols (Yochem et al., 2000; Yochem, 2006).

Expression analysis and DNA constructs.

To generate P_{fbn-1}::GFP-PEST, nucleotides 7621743–7625323 of Chromosome III were amplified from N2 and spliced to the *gfp-pest* cassette from pAF207 (Frand et al., 2005) using PCR methods. We note that strains expressing P_{fbn-1}::GFP-PEST also contain a P_{ttx-3}::GFP marker, which is expressed in AIY neurons but not in epidermal cells (Hobert et al., 1997). To generate the mini-*fbn-1*::mCherry (*fbn-1*Δ49-2418::mCherry) fusion gene, nucleotides 7621652–7626214 of Chromosome III, which contain the presumptive *fbn-1* promoter and first 48 codons, were amplified from N2 DNA and cloned into pUC19. Then nucleotides 7638794–7641181 of Chromosome III, which contain the last 362 codons and native 3' UTR of *fbn-1*, were amplified from N2 and inserted downstream of the former fragment, producing plasmid pVM61. The mCherry cassette from KP1272 was then inserted in-frame between the two genomic fragments using an engineered NotI site. Injection of DNA constructs or PCR products to generate extrachromosomal arrays was carried out using standard procedures (Mello and Fire, 1995).

A rescuing *fbn-1* cDNA sequence was PCR amplified as three overlapping fragments (atgtctac...gaaaattg, 2049 bp; ggaaaagt...gtacctgc, 3581 bp; gtatggct...gattctag, 2758 bp) from a cDNA library (gift of Carl Procko) and the plasmid clone yk670d9 (gift of Yuji Kohara), which were then assembled into a single 8065-bp cDNA sequence using internal PstI and SalI sites (at position 1985 bp and 5431 bp, respectively). A 4406-bp *fbn-1* promoter sequence capable of driving embryonic GFP expression was isolated

977 (tcgaggag...ttgcagga) and assembled with the *fbn-1* cDNA as a SbfI-AgeI promoter
978 fragment and an AgeI-NheI cDNA fragment in a modified pPD95.69 vector bearing an
979 NheI-SpeI unc-54 3'UTR fragment, to create the plasmid pMH281.
980
981 **Microscopy.**
982 With the exception of FRET studies, micrographs were taken with a Nikon Eclipse
983 microscope, using a 100× objective. Percent Pin was calculated by counting 1.5-fold or
984 older embryos or L1-stage larvae. Fluorescent confocal images were acquired using a
985 100× objective on an Olympus IX-71 inverted microscope. Image acquisition and
986 microscope control were carried out with Metamorph software (Molecular Devices).
987
988 Keyhole/sensory depression depth was quantified using Openlab software. Keyhole
989 depth for *mec-8; sym-3* embryos grown on *let-502* RNAi plates was quantified every 15
990 min starting at the late comma stage through the 3-fold stage. *mec-8; sqt-3* embryo
991 keyhole depth was measured by growing embryos at 25°C starting at the 2-fold stage
992 and quantified every 60 min for 5 hr.
993
994 **Trypsin treatment of embryos.**
995 Embryos were obtained by bleaching N2 adults, using standard methods. Embryos
996 were permeabilized by treatment with 2 mg/ml chitinase for 5–10 min at room
997 temperature (Bianchi and Driscoll, 2006). Permeabilized mixed-stage embryos were
998 treated with trypsin (Sigma Aldrich) at a concentration of 5 μg/ml for 15 min at room

temperature followed by trypsin inhibitor (Sigma Aldrich), which was added to a concentration of 50 μg/ml and incubated for 2 min (Priess and Hirsh, 1986). Embryos were rinsed with M9 and examined immediately using DIC microscopy.

ACKNOWLEDGEMENTS

Some strains were provided by the *Caenorhabditis* Genetics Center (CGC), which is funded by the US National Institutes of Health (NIH) Office of Research Infrastructure Programs (P40 OD010440). We also thank the National BioResource Project of Japan and Eric Jorgensen for strains. FRET imaging was conducted in the Cell Sciences Imaging Facility at Stanford, which is supported by award S10RR02557401 from the National Center for Research Resources. MBG and MK were supported by NIH grants NS047715, EB006745 and 1K99NS089942-01 as well as by a Human Frontier Science Program Long-Term Fellowship (MK), respectively. AC and MC were supported by NIH grant GM30997. AC was also supported by FONDECYT grant 1131038. AF and VM were supported by the NMF and ACS (RSG-12-149-01-DCC). SS and MH were supported in part by NIH grants NS073121and NS064273. MH was also supported in part by NIH grant GM108754. Support at the University of Wyoming was from the NIH (R01 grant GM066868 to DSF and INBRE grant P20 GM103432). We thank Amy Fluet for editing, Dan Starr for valuable scientific input, and Ronald Tepper for help with the microarray data analysis.

COMPETING INTERESTS

The authors of this manuscript have no competing interests as defined by the International committee of Medical Journal Editors.

REFERENCES

Ahringer, J., ed. Reverse genetics (April 6, 2006), *WormBook*, ed. The *C. elegans* Research Community, WormBook, doi/10.1895/wormbook.1.47.1, http://www.wormbook.org.

Ai, E., Poole, D. S. and Skop, A. R. (2009). RACK-1 directs dynactin-dependent RAB-11 endosomal recycling during mitosis in Caenorhabditis elegans. *Mol Biol Cell* **20**, 1629-1638.

Ashworth, J. L., Kelly, V., Rock, M. J., Shuttleworth, C. A. and Kielty, C. M. (1999). Regulation of fibrillin carboxy-terminal furin processing by N-glycosylation, and association of amino- and carboxy-terminal sequences. *J Cell Sci* **112 (Pt 22)**, 4163-4171.

Baldwin, A. K., Simpson, A., Steer, R., Cain, S. A. and Kielty, C. M. (2013). Elastic fibres in health and disease. *Expert Rev Mol Med* **15**, e8.

Barstead, R., G, M., B, C. and al., e. (2012). large-scale screening for targeted knockouts in the Caenorhabditis elegans genome. *G3 (Bethesda)* **2**, 1415-1425.

Baum, P. D. and Garriga, G. (1997). Neuronal migrations and axon fasciculation are disrupted in ina-1 integrin mutants. *Neuron* **19**, 51-62.

Beitel, G. J. and Krasnow, M. A. (2000). Genetic control of epithelial tube size in the Drosophila tracheal system. *Development* **127**, 3271-3282.

Bellen, H. J., Kooyer, S., D'Evelyn, D. and Pearlman, J. (1992a). The Drosophila couch potato protein is expressed in nuclei of peripheral neuronal precursors and shows homology to RNA-binding proteins. *Genes Dev* **6**, 2125-2136.

Bellen, H. J., Vaessin, H., Bier, E., Kolodkin, A., D'Evelyn, D., Kooyer, S. and Jan, Y. N. (1992b). The Drosophila couch potato gene: an essential gene required for normal adult behavior. *Genetics* **131**, 365-375.

Bembenek, J. N., White, J. G. and Zheng, Y. (2010). A role for separase in the regulation of RAB-11-positive vesicles at the cleavage furrow and midbody. *Curr Biol* **20**, 259-264.

Berney, C. and Danuser, G. (2003). FRET or no FRET: a quantitative comparison. *Biophys J* **84**, 3992-4010.

Bianchi, L. and Driscoll, M. Culture of embryonic *C. elegans* cells for electrophysiological and pharmacological analyses (September 30, 2006), *WormBook*, ed. The *C. elegans* Research Community, WormBook, doi/10.1895/wormbook.1.122.1, http://www.wormbook.org.

Biery, N. J., Eldadah, Z. A., Moore, C. S., Stetten, G., Spencer, F. and Dietz, H. C. (1999). Revised genomic organization of FBN1 and significance for regulated gene expression. *Genomics* **56**, 70-77.

Blethrow, J., Zhang, C., Shokat, K. M. and Weiss, E. L. (2004). Design and use of analog-sensitive protein kinases. *Curr Protoc Mol Biol* **Chapter 18**, Unit 18 11.

Borghi, N., Sorokina, M., Shcherbakova, O. G., Weis, W. I., Pruitt, B. L., Nelson, W. J. and Dunn, A. R. (2012). E-cadherin is under constitutive actomyosin-generated tension that is increased at cell-cell contacts upon externally applied stretch. *Proc Natl Acad Sci U S A* **109**, 12568-12573.

Bosher, J. M., Hahn, B. S., Legouis, R., Sookhareea, S., Weimer, R. M., Gansmuller, A., Chisholm, A. D., Rose, A. M., Bessereau, J. L. and Labouesse, M. (2003). The Caenorhabditis elegans vab-10 spectraplakin isoforms protect the epidermis against internal and external forces. *J Cell Biol* **161**, 757-768.

Bretscher, A. (1991). Microfilament structure and function in the cortical cytoskeleton. *Annu Rev Cell Biol* **7**, 337-374.

Brown, N. H. (2011). Extracellular matrix in development: insights from mechanisms conserved between invertebrates and vertebrates. *Cold Spring Harb Perspect Biol* **3**.

Burchett, M. E., Ling, I. F. and Estus, S. (2011). FBN1 isoform expression varies in a tissue and development-specific fashion. *Biochem Biophys Res Commun* **411**, 323-328.

Bussey, H., Andrews, B. and Boone, C. (2006). From worm genetic networks to complex human diseases. *Nat Genet* **38**, 862-863.

Cai, D., Chen, S. C., Prasad, M., He, L., Wang, X., Choesmel-Cadamuro, V., Sawyer, J. K., Danuser, G. and Montell, D. J. (2014). Mechanical feedback through E-cadherin promotes direction sensing during collective cell migration. *Cell* **157**, 1146-1159.

Calixto, A., Ma, C. and Chalfie, M. (2010). Conditional gene expression and RNAi using MEC-8-dependent splicing in C. elegans. *Nat Methods* **7**, 407-411.

Campelo, F. and Malhotra, V. (2012). Membrane fission: the biogenesis of transport carriers. *Annu Rev Biochem* **81**, 407-427.

Chen, W., Feng, Y., Chen, D. and Wandinger-Ness, A. (1998). Rab11 is required for trans-golgi network-to-plasma membrane transport and a preferential target for GDP dissociation inhibitor. *Mol Biol Cell* **9**, 3241-3257.

Chen, Y. and Periasamy, A. (2006). Intensity range based quantitative FRET data analysis to localize protein molecules in live cell nuclei. *J Fluoresc* **16**, 95-104.

Cheng, H., Govindan, J. A. and Greenstein, D. (2008). Regulated trafficking of the MSP/Eph receptor during oocyte meiotic maturation in C. elegans. *Curr Biol* **18**, 705-714.

Chisholm, A.D. and Hardin, J. Epidermal morphogenesis (December 01, 2005), *WormBook*, ed. The *C. elegans* Research Community, WormBook, doi/10.1895/wormbook.1.35.1 , http://www.wormbook.org.

Chisholm, A. D. and Hsiao, T. I. (2012). The Caenorhabditis elegans epidermis as a model skin. I: development, patterning, and growth. *Wiley Interdiscip Rev Dev Biol* **1**, 861-878.

Conway, D. E., Breckenridge, M. T., Hinde, E., Gratton, E., Chen, C. S. and Schwartz, M. A. (2013). Fluid shear stress on endothelial cells modulates mechanical tension across VE-cadherin and PECAM-1. *Curr Biol* **23**, 1024-1030.

Corson, G. M., Chalberg, S. C., Dietz, H. C., Charbonneau, N. L. and Sakai, L. Y. (1993). Fibrillin binds calcium and is coded by cDNAs that reveal a multidomain structure and alternatively spliced exons at the 5' end. *Genomics* **17**, 476-484.

Corson, G. M., Charbonneau, N. L., Keene, D. R. and Sakai, L. Y. (2004). Differential expression of fibrillin-3 adds to microfibril variety in human and avian, but not rodent, connective tissues. *Genomics* **83**, 461-472.

Costa, M., Draper, B. W. and Priess, J. R. (1997). The role of actin filaments in patterning the Caenorhabditis elegans cuticle. *Dev Biol* **184**, 373-384.
Cowling, B. S., Toussaint, A., Muller, J. and Laporte, J. (2012). Defective membrane remodeling in neuromuscular diseases: insights from animal models. *PLoS Genet* **8**, e1002595.
Davidson, L. A. (2011). Embryo mechanics: balancing force production with elastic resistance during morphogenesis. *Curr Top Dev Biol* **95**, 215-241.
---- (2012). Epithelial machines that shape the embryo. *Trends Cell Biol* **22**, 82-87.
Davies, A. G., Spike, C. A., Shaw, J. E. and Herman, R. K. (1999). Functional overlap between the mec-8 gene and five sym genes in Caenorhabditis elegans. *Genetics* **153**, 117-134.
Davis, C. G. (1990). The many faces of epidermal growth factor repeats. *New Biol* **2**, 410-419.
Day, R. N., Booker, C. F. and Periasamy, A. (2008). Characterization of an improved donor fluorescent protein for Forster resonance energy transfer microscopy. *J Biomed Opt* **13**, 031203.
Denholm, B. and Skaer, H. (2003). Tubulogenesis: a role for the apical extracellular matrix? *Curr Biol* **13**, R909-911.
Dietz, H. C., Loeys, B., Carta, L. and Ramirez, F. (2005). Recent progress towards a molecular understanding of Marfan syndrome. *Am J Med Genet C Semin Med Genet* **139C**, 4-9.
Dong, B., Hannezo, E. and Hayashi, S. (2014). Balance between apical membrane growth and luminal matrix resistance determines epithelial tubule shape. *Cell Rep* **7**, 941-950.
Epstein, C. J., Erickson, R. P. and Wynshaw-Boris, A. (2004). *Inborn Errors of Development: The Molecular Basis of Clinical Disorders of Morphogenesis (2004). Ed. Epstein, C. J., Erickson, R. P., Wynshaw-Boris, A. Oxford Momographs on Mecial Genetics, 49. New York, USA. Oxford University Press*. New York: Oxford University Press.
Fay, D. S., Polley, S. R., Kuang, J., Kuzmanov, A., Hazel, J. W., Mani, K., Veo, B. L. and Yochem, J. (2012). A regulatory module controlling pharyngeal development and function in Caenorhabditis elegans. *Genetics* **191**, 827-843.
Fay, D. S., Qiu, X., Large, E., Smith, C. P., Mango, S. and Johanson, B. L. (2004). The coordinate regulation of pharyngeal development in C. elegans by lin-35/Rb, pha-1, and ubc-18. *Dev Biol* **271**, 11-25.
Frand, A. R., Russel, S. and Ruvkun, G. (2005). Functional genomic analysis of C. elegans molting. *PLoS Biol* **3**, e312.
Glasscock, E. and Tanouye, M. A. (2005). Drosophila couch potato mutants exhibit complex neurological abnormalities including epilepsy phenotypes. *Genetics* **169**, 2137-2149.
Grant, B. D. and Donaldson, J. G. (2009). Pathways and mechanisms of endocytic recycling. *Nat Rev Mol Cell Biol* **10**, 597-608.

Grashoff, C., Hoffman, B. D., Brenner, M. D., Zhou, R., Parsons, M., Yang, M. T., McLean, M. A., Sligar, S. G., Chen, C. S., Ha, T., et al. (2010). Measuring mechanical tension across vinculin reveals regulation of focal adhesion dynamics. *Nature* **466**, 263-266.

Guillot, C. and Lecuit, T. (2013). Mechanics of epithelial tissue homeostasis and morphogenesis. *Science* **340**, 1185-1189.

Guruharsha, K. G., Rual, J. F., Zhai, B., Mintseris, J., Vaidya, P., Vaidya, N., Beekman, C., Wong, C., Rhee, D. Y., Cenaj, O., et al. (2011). A protein complex network of Drosophila melanogaster. *Cell* **147**, 690-703.

Hales, C. M., Vaerman, J. P. and Goldenring, J. R. (2002). Rab11 family interacting protein 2 associates with Myosin Vb and regulates plasma membrane recycling. *J Biol Chem* **277**, 50415-50421.

Hammarlund, M., Davis, W. S. and Jorgensen, E. M. (2000). Mutations in beta-spectrin disrupt axon outgrowth and sarcomere structure. *J Cell Biol* **149**, 931-942.

Hammarlund, M., Jorgensen, E. M. and Bastiani, M. J. (2007). Axons break in animals lacking beta-spectrin. *J Cell Biol* **176**, 269-275.

He, H., Wang, J., Liu, T., Liu, X. S., Li, T., Wang, Y., Qian, Z., Zheng, H., Zhu, X., Wu, T., et al. (2007). Mapping the C. elegans noncoding transcriptome with a whole-genome tiling microarray. *Genome Res* **17**, 1471-1477.

Heiman, M. G. and Shaham, S. (2009). DEX-1 and DYF-7 establish sensory dendrite length by anchoring dendritic tips during cell migration. *Cell* **137**, 344-355.

Heisenberg, C. P. and Bellaiche, Y. (2013). Forces in tissue morphogenesis and patterning. *Cell* **153**, 948-962.

Herman, R. K. and Yochem, J. Genetic enhancers (September 16, 2005), *WormBook*, ed. The *C. elegans* Research Community, WormBook, doi/10.1895/wormbook.1.27.1, http://www.wormbook.org.

Hobert, O., Mori, I., Yamashita, Y., Honda, H., Ohshima, Y., Liu, Y. and Ruvkun, G. (1997). Regulation of interneuron function in the C. elegans thermoregulatory pathway by the ttx-3 LIM homeobox gene. *Neuron* **19**, 345-357.

Horgan, C. P., Hanscom, S. R., Jolly, R. S., Futter, C. E. and McCaffrey, M. W. (2010). Rab11-FIP3 links the Rab11 GTPase and cytoplasmic dynein to mediate transport to the endosomal-recycling compartment. *J Cell Sci* **123**, 181-191.

Hresko, M. C., Schriefer, L. A., Shrimankar, P. and Waterston, R. H. (1999). Myotactin, a novel hypodermal protein involved in muscle-cell adhesion in Caenorhabditis elegans. *J Cell Biol* **146**, 659-672.

Hynes, R. O. (2009). The extracellular matrix: not just pretty fibrils. *Science* **326**, 1216-1219.

Jazwinska, A., Ribeiro, C. and Affolter, M. (2003). Epithelial tube morphogenesis during Drosophila tracheal development requires Piopio, a luminal ZP protein. *Nat Cell Biol* **5**, 895-901.

Judd, K. P. (1984). Hyperelasticity syndromes. *Cutis* **33**, 494-496.

Keller, R., Davidson, L. A. and Shook, D. R. (2003). How we are shaped: the biomechanics of gastrulation. *Differentiation* **71**, 171-205.

Keller, R., Shook, D. and Skoglund, P. (2008). The forces that shape embryos: physical aspects of convergent extension by cell intercalation. *Phys Biol* **5**, 015007.
Kelly, E. E., Horgan, C. P. and McCaffrey, M. W. (2012). Rab11 proteins in health and disease. *Biochem Soc Trans* **40**, 1360-1367.
King, C., Sarabipour, S., Byrne, P., Leahy, D. J. and Hristova, K. (2014). The FRET signatures of noninteracting proteins in membranes: simulations and experiments. *Biophys J* **106**, 1309-1317.
Koppen, M., Simske, J. S., Sims, P. A., Firestein, B. L., Hall, D. H., Radice, A. D., Rongo, C. and Hardin, J. D. (2001). Cooperative regulation of AJM-1 controls junctional integrity in Caenorhabditis elegans epithelia. *Nat Cell Biol* **3**, 983-991.
Krieg, M., Dunn, A. R. and Goodman, M. B. (2014). Mechanical control of the sense of touch by beta-spectrin. *Nat Cell Biol* **16**, 224-233.
Kusch, M. and Edgar, R. S. (1986). Genetic studies of unusual loci that affect body shape of the nematode Caenorhabditis elegans and may code for cuticle structural proteins. *Genetics* **113**, 621-639.
Kuzmanov, A., Yochem, J. and Fay, D. S. (2014). Analysis of PHA-1 Reveals a Limited Role in Pharyngeal Development and Novel Functions in Other Tissues. *Genetics*.
Labouesse, M. (2012). Role of the extracellular matrix in epithelial morphogenesis: a view from C. elegans. *Organogenesis* **8**, 65-70.
Lane, M. C., Koehl, M. A., Wilt, F. and Keller, R. (1993). A role for regulated secretion of apical extracellular matrix during epithelial invagination in the sea urchin. *Development* **117**, 1049-1060.
Lehner, B., Calixto, A., Crombie, C., Tischler, J., Fortunato, A., Chalfie, M. and Fraser, A. G. (2006). Loss of LIN-35, the Caenorhabditis elegans ortholog of the tumor suppressor p105Rb, results in enhanced RNA interference. *Genome Biol* **7**, R4.
Liu, O. W. and Shen, K. (2012). The transmembrane LRR protein DMA-1 promotes dendrite branching and growth in C. elegans. *Nat Neurosci* **15**, 57-63.
Lonnqvist, L., Reinhardt, D., Sakai, L. and Peltonen, L. (1998). Evidence for furin-type activity-mediated C-terminal processing of profibrillin-1 and interference in the processing by certain mutations. *Hum Mol Genet* **7**, 2039-2044.
Lundquist, E. A., Herman, R. K., Rogalski, T. M., Mullen, G. P., Moerman, D. G. and Shaw, J. E. (1996). The mec-8 gene of C. elegans encodes a protein with two RNA recognition motifs and regulates alternative splicing of unc-52 transcripts. *Development* **122**, 1601-1610.
Luschnig, S. and Uv, A. (2014). Luminal matrices: an inside view on organ morphogenesis. *Exp Cell Res* **321**, 64-70.
Mammoto, A., Ohtsuka, T., Hotta, I., Sasaki, T. and Takai, Y. (1999). Rab11BP/Rabphilin-11, a downstream target of rab11 small G protein implicated in vesicle recycling. *J Biol Chem* **274**, 25517-25524.
Mancuso, V. P., Parry, J. M., Storer, L., Poggioli, C., Nguyen, K. C., Hall, D. H. and Sundaram, M. V. (2012). Extracellular leucine-rich repeat proteins are required to organize the apical extracellular matrix and maintain epithelial junction integrity in C. elegans. *Development* **139**, 979-990.

Mango, S. E. (2001). Stop making nonSense: the C. elegans smg genes. *Trends Genet* **17**, 646-653.
McLachlan, I. G. and Heiman, M. G. (2013). Shaping dendrites with machinery borrowed from epithelia. *Curr Opin Neurobiol* **23**, 1005-1010.
Mello, C. and Fire, A. (1995). DNA transformation. *Methods Cell Biol* **48**, 451-482.
Meng, F., Suchyna, T. M., Lazakovitch, E., Gronostajski, R. M. and Sachs, F. (2011). Real Time FRET Based Detection of Mechanical Stress in Cytoskeletal and Extracellular Matrix Proteins. *Cell Mol Bioeng* **4**, 148-159.
Meng, F., Suchyna, T. M. and Sachs, F. (2008). A fluorescence energy transfer-based mechanical stress sensor for specific proteins in situ. *FEBS J* **275**, 3072-3087.
Milewicz, D. M., Urban, Z. and Boyd, C. (2000). Genetic disorders of the elastic fiber system. *Matrix Biol* **19**, 471-480.
Mockler, T. C., Chan, S., Sundaresan, A., Chen, H., Jacobsen, S. E. and Ecker, J. R. (2005). Applications of DNA tiling arrays for whole-genome analysis. *Genomics* **85**, 1-15.
Moore, K. L., Persaud, T. V. N. and Torchia, M. G. (2013). Before we are born: Essentials of embryology and birth defects.
Moorthy, S., Chen, L. and Bennett, V. (2000). Caenorhabditis elegans beta-G spectrin is dispensable for establishment of epithelial polarity, but essential for muscular and neuronal function. *J Cell Biol* **149**, 915-930.
Morimatsu, M., Mekhdjian, A. H., Adhikari, A. S. and Dunn, A. R. (2013). Molecular tension sensors report forces generated by single integrin molecules in living cells. *Nano Lett* **13**, 3985-3989.
Moussian, B., Veerkamp, J., Muller, U. and Schwarz, H. (2007). Assembly of the Drosophila larval exoskeleton requires controlled secretion and shaping of the apical plasma membrane. *Matrix Biol* **26**, 337-347.
Norman, K. R. and Moerman, D. G. (2002). Alpha spectrin is essential for morphogenesis and body wall muscle formation in Caenorhabditis elegans. *J Cell Biol* **157**, 665-677.
Paszek, M. J., DuFort, C. C., Rossier, O., Bainer, R., Mouw, J. K., Godula, K., Hudak, J. E., Lakins, J. N., Wijekoon, A. C., Cassereau, L., et al. (2014). The cancer glycocalyx mechanically primes integrin-mediated growth and survival. *Nature* **511**, 319-325.
Perkins, L. A., Hedgecock, E. M., Thomson, J. N. and Culotti, J. G. (1986). Mutant sensory cilia in the nematode Caenorhabditis elegans. *Dev Biol* **117**, 456-487.
Peter, B. J., Kent, H. M., Mills, I. G., Vallis, Y., Butler, P. J., Evans, P. R. and McMahon, H. T. (2004). BAR domains as sensors of membrane curvature: the amphiphysin BAR structure. *Science* **303**, 495-499.
Pickett, F. B. and Meeks-Wagner, D. R. (1995). Seeing double: appreciating genetic redundancy. *Plant Cell* **7**, 1347-1356.
Piha-Gossack, A., Sossin, W. and Reinhardt, D. P. (2012). The evolution of extracellular fibrillins and their functional domains. *PLoS One* **7**, e33560.
Plaza, S., Chanut-Delalande, H., Fernandes, I., Wassarman, P. M. and Payre, F. (2010). From A to Z: apical structures and zona pellucida-domain proteins. *Trends Cell Biol* **20**, 524-532.

Portereiko, M. F. and Mango, S. E. (2001). Early morphogenesis of the Caenorhabditis elegans pharynx. *Dev Biol* **233**, 482-494.
Priess, J. R. and Hirsh, D. I. (1986). Caenorhabditis elegans morphogenesis: the role of the cytoskeleton in elongation of the embryo. *Dev Biol* **117**, 156-173.
Qadota, H., Inoue, M., Hikita, T., Koppen, M., Hardin, J. D., Amano, M., Moerman, D. G. and Kaibuchi, K. (2007). Establishment of a tissue-specific RNAi system in C. elegans. *Gene* **400**, 166-173.
Ramani, A. K., Calarco, J. A., Pan, Q., Mavandadi, S., Wang, Y., Nelson, A. C., Lee, L. J., Morris, Q., Blencowe, B. J., Zhen, M., et al. (2011). Genome-wide analysis of alternative splicing in Caenorhabditis elegans. *Genome Res* **21**, 342-348.
Ramirez, F. and Dietz, H. C. (2009). Extracellular microfibrils in vertebrate development and disease processes. *J Biol Chem* **284**, 14677-14681.
Ramirez, F. and Sakai, L. Y. (2010). Biogenesis and function of fibrillin assemblies. *Cell Tissue Res* **339**, 71-82.
Ren, M., Xu, G., Zeng, J., De Lemos-Chiarandini, C., Adesnik, M. and Sabatini, D. D. (1998). Hydrolysis of GTP on rab11 is required for the direct delivery of transferrin from the pericentriolar recycling compartment to the cell surface but not from sorting endosomes. *Proc Natl Acad Sci U S A* **95**, 6187-6192.
Rifkin, D. B. (2005). Latent transforming growth factor-beta (TGF-beta) binding proteins: orchestrators of TGF-beta availability. *J Biol Chem* **280**, 7409-7412.
Roch, F., Alonso, C. R. and Akam, M. (2003). Drosophila miniature and dusky encode ZP proteins required for cytoskeletal reorganisation during wing morphogenesis. *J Cell Sci* **116**, 1199-1207.
Rogalski, T. M., Williams, B. D., Mullen, G. P. and Moerman, D. G. (1993). Products of the unc-52 gene in Caenorhabditis elegans are homologous to the core protein of the mammalian basement membrane heparan sulfate proteoglycan. *Genes Dev* **7**, 1471-1484.
Sakagami, H., Sanda, M., Fukaya, M., Miyazaki, T., Sukegawa, J., Yanagisawa, T., Suzuki, T., Fukunaga, K., Watanabe, M. and Kondo, H. (2008). IQ-ArfGEF/BRAG1 is a guanine nucleotide exchange factor for Arf6 that interacts with PSD-95 at postsynaptic density of excitatory synapses. *Neurosci Res* **60**, 199-212.
Saleh, M. C., van Rij, R. P., Hekele, A., Gillis, A., Foley, E., O'Farrell, P. H. and Andino, R. (2006). The endocytic pathway mediates cell entry of dsRNA to induce RNAi silencing. *Nat Cell Biol* **8**, 793-802.
Sato, M., Grant, B. D., Harada, A. and Sato, K. (2008). Rab11 is required for synchronous secretion of chondroitin proteoglycans after fertilization in Caenorhabditis elegans. *J Cell Sci* **121**, 3177-3186.
Satoh, A. K., O'Tousa, J. E., Ozaki, K. and Ready, D. F. (2005). Rab11 mediates post-Golgi trafficking of rhodopsin to the photosensitive apical membrane of Drosophila photoreceptors. *Development* **132**, 1487-1497.
Schmidt, P. S., Zhu, C. T., Das, J., Batavia, M., Yang, L. and Eanes, W. F. (2008). An amino acid polymorphism in the couch potato gene forms the basis for climatic adaptation in Drosophila melanogaster. *Proc Natl Acad Sci U S A* **105**, 16207-16211.

Schnabel, H. and Schnabel, R. (1990). An Organ-Specific Differentiation Gene, pha-1, from Caenorhabditis elegans. *Science* **250**, 686-688.

Shi, A., Chen, C. C., Banerjee, R., Glodowski, D., Audhya, A., Rongo, C. and Grant, B. D. (2010). EHBP-1 functions with RAB-10 during endocytic recycling in Caenorhabditis elegans. *Mol Biol Cell* **21**, 2930-2943.

Shimamoto, A., Kitao, S., Ichikawa, K., Suzuki, N., Yamabe, Y., Imamura, O., Tokutake, Y., Satoh, M., Matsumoto, T., Kuromitsu, J., et al. (1996). A unique human gene that spans over 230 kb in the human chromosome 8p11-12 and codes multiple family proteins sharing RNA-binding motifs. *Proc Natl Acad Sci U S A* **93**, 10913-10917.

Simmer, F., Tijsterman, M., Parrish, S., Koushika, S. P., Nonet, M. L., Fire, A., Ahringer, J. and Plasterk, R. H. (2002). Loss of the putative RNA-directed RNA polymerase RRF-3 makes C. elegans hypersensitive to RNAi. *Curr Biol* **12**, 1317-1319.

Spike, C. A., Davies, A. G., Shaw, J. E. and Herman, R. K. (2002). MEC-8 regulates alternative splicing of unc-52 transcripts in C. elegans hypodermal cells. *Development* **129**, 4999-5008.

Stiernagle, T. Maintenance of *C. elegans* (February 11, 2006), *WormBook*, ed. The *C. elegans* Research Community, WormBook, doi/10.1895/wormbook.1.101.1, http://www.wormbook.org.

Sulston, J. E., Schierenberg, E., White, J. G. and Thomson, J. N. (1983). The embryonic cell lineage of the nematode Caenorhabditis elegans. *Dev Biol* **100**, 64-119.

Swanson, L. E., Yu, M., Nelson, K. S., Laprise, P., Tepass, U. and Beitel, G. J. (2009). Drosophila convoluted/dALS is an essential gene required for tracheal tube morphogenesis and apical matrix organization. *Genetics* **181**, 1281-1290.

Syed, Z. A., Bouge, A. L., Byri, S., Chavoshi, T. M., Tang, E., Bouhin, H., van Dijk-Hard, I. F. and Uv, A. (2012). A luminal glycoprotein drives dose-dependent diameter expansion of the Drosophila melanogaster hindgut tube. *PLoS Genet* **8**, e1002850.

Takahashi, S., Kubo, K., Waguri, S., Yabashi, A., Shin, H. W., Katoh, Y. and Nakayama, K. (2012). Rab11 regulates exocytosis of recycling vesicles at the plasma membrane. *J Cell Sci* **125**, 4049-4057.

Tautz, D. (2000). A genetic uncertainty problem. *Trends Genet* **16**, 475-477.

Thomas, J. H. (1993). Thinking about genetic redundancy. *Trends Genet* **9**, 395-399.

Timmons, L., Court, D. L. and Fire, A. (2001). Ingestion of bacterially expressed dsRNAs can produce specific and potent genetic interference in Caenorhabditis elegans. *Gene* **263**, 103-112.

Todorovic, V., Jurukovski, V., Chen, Y., Fontana, L., Dabovic, B. and Rifkin, D. B. (2005). Latent TGF-beta binding proteins. *Int J Biochem Cell Biol* **37**, 38-41.

Tucker, M. and Han, M. (2008). Muscle cell migrations of C. elegans are mediated by the alpha-integrin INA-1, Eph receptor VAB-1, and a novel peptidase homologue MNP-1. *Dev Biol* **318**, 215-223.

Ullrich, O., Reinsch, S., Urbe, S., Zerial, M. and Parton, R. G. (1996). Rab11 regulates recycling through the pericentriolar recycling endosome. *J Cell Biol* **135**, 913-924.

Urbe, S., Huber, L. A., Zerial, M., Tooze, S. A. and Parton, R. G. (1993). Rab11, a small GTPase associated with both constitutive and regulated secretory pathways in PC12 cells. *FEBS Lett* **334**, 175-182.

von Kalm, L., Fristrom, D. and Fristrom, J. (1995). The making of a fly leg: a model for epithelial morphogenesis. *Bioessays* **17**, 693-702.

Wang, D., Kennedy, S., Conte, D., Jr., Kim, J. K., Gabel, H. W., Kamath, R. S., Mello, C. C. and Ruvkun, G. (2005). Somatic misexpression of germline P granules and enhanced RNA interference in retinoblastoma pathway mutants. *Nature* **436**, 593-597.

Ward, E. S., Martinez, C., Vaccaro, C., Zhou, J., Tang, Q. and Ober, R. J. (2005). From sorting endosomes to exocytosis: association of Rab4 and Rab11 GTPases with the Fc receptor, FcRn, during recycling. *Mol Biol Cell* **16**, 2028-2038.

Wehman, A. M., Poggioli, C., Schweinsberg, P., Grant, B. D. and Nance, J. (2011). The P4-ATPase TAT-5 inhibits the budding of extracellular vesicles in C. elegans embryos. *Curr Biol* **21**, 1951-1959.

Welz, T., Wellbourne-Wood, J. and Kerkhoff, E. (2014). Orchestration of cell surface proteins by Rab11. *Trends Cell Biol* **24**, 407-415.

Wilcke, M., Johannes, L., Galli, T., Mayau, V., Goud, B. and Salamero, J. (2000). Rab11 regulates the compartmentalization of early endosomes required for efficient transport from early endosomes to the trans-golgi network. *J Cell Biol* **151**, 1207-1220.

Wilkin, M. B., Becker, M. N., Mulvey, D., Phan, I., Chao, A., Cooper, K., Chung, H. J., Campbell, I. D., Baron, M. and MacIntyre, R. (2000). Drosophila dumpy is a gigantic extracellular protein required to maintain tension at epidermal-cuticle attachment sites. *Curr Biol* **10**, 559-567.

Willenborg, C. and Prekeris, R. (2011). Apical protein transport and lumen morphogenesis in polarized epithelial cells. *Biosci Rep* **31**, 245-256.

Williams, B. D. and Waterston, R. H. (1994). Genes critical for muscle development and function in Caenorhabditis elegans identified through lethal mutations. *J Cell Biol* **124**, 475-490.

Wissmann, A., Ingles, J. and Mains, P. E. (1999). The Caenorhabditis elegans mel-11 myosin phosphatase regulatory subunit affects tissue contraction in the somatic gonad and the embryonic epidermis and genetically interacts with the Rac signaling pathway. *Dev Biol* **209**, 111-127.

Wissmann, A., Ingles, J., McGhee, J. D. and Mains, P. E. (1997). Caenorhabditis elegans LET-502 is related to Rho-binding kinases and human myotonic dystrophy kinase and interacts genetically with a homolog of the regulatory subunit of smooth muscle myosin phosphatase to affect cell shape. *Genes Dev* **11**, 409-422.

Yochem, J., Bell, L. R. and Herman, R. K. (2004). The identities of sym-2, sym-3 and sym-4, three genes that are synthetically lethal with mec-8 in Caenorhabditis elegans. *Genetics* **168**, 1293-1306.

Yochem, J., Gu, T. and Han, M. (1998). A new marker for mosaic analysis in Caenorhabditis elegans indicates a fusion between hyp6 and hyp7, two major components of the hypodermis. *Genetics* **149**, 1323-1334.

Yochem, J. and Herman, R. K. Genetic mosaics (December 27, 2005), *WormBook*, ed. The *C. elegans* Research Community, WormBook, doi/10.1895/wormbook.1.58.1, http://www.wormbook.org.

Yochem, J., Sundaram, M. and Bucher, E. A. (2000). Mosaic analysis in Caenorhabditis elegans. *Methods Mol Biol* **135**, 447-462.

Yochem, J. Nomarski images for learning the anatomy, with tips for mosaic analysis (January 24, 2006), *WormBook*, ed. The *C. elegans* Research Community, WormBook, doi/10.1895/wormbook.1.100.1, http://www.wormbook.org.

Zeng, J., Ren, M., Gravotta, D., De Lemos-Chiarandini, C., Lui, M., Erdjument-Bromage, H., Tempst, P., Xu, G., Shen, T. H., Morimoto, T., et al. (1999). Identification of a putative effector protein for rab11 that participates in transferrin recycling. *Proc Natl Acad Sci U S A* **96**, 2840-2845.

Zhang, D. and Aravind, L. (2010). Identification of novel families and classification of the C2 domain superfamily elucidate the origin and evolution of membrane targeting activities in eukaryotes. *Gene* **469**, 18-30.

Zhang, Y., Foster, J. M., Nelson, L. S., Ma, D. and Carlow, C. K. (2005). The chitin synthase genes chs-1 and chs-2 are essential for C. elegans development and responsible for chitin deposition in the eggshell and pharynx, respectively. *Dev Biol* **285**, 330-339.

FIGURE LEGENDS

Figure 1. *mec-8; sym-3* and *mec-8; sym-4* mutants exhibit an abnormal ingression of the anterior epidermis. (A) Whereas wild-type 1.5-fold embryos display only a shallow ingression of the anterior epidermis (sensory depression) and little or no ingression by the 3-fold stage, *mec-8; sym-3* and *mec-8; sym-4* (data not shown) mutants contain a deep keyhole-shaped ingression that increases in depth between the 1.5- and 3-fold stages. *mec-8; sym-3* and *mec-8; sym-4* (data not shown) L1 larvae also contain an ingressed pharynx (Pin) and associated deformities in the head region. Yellow dashed lines indicate lateral pharyngeal borders; orange dashed lines, the sensory depression or keyhole; black arrows, posterior extent of ingression. White scale bars = 10 μm, black bars = 5 μm. (B) Quantification of the Pin phenotype in single and double mutants and in *mec-8; sym-4* double mutants containing multi-copy extrachromosomal arrays (*fdEx251* and *fdEx254*) that express the *fbn-1e* cDNA isoform under the control of the native *fbn-1* promoter. Error bars represent 95% CIs. For additional details, see Table 1 and Supplementary File 1. (C) Spring-and-cylinder model in which the pharynx exerts an inward-pulling force at the anterior epidermis throughout the mid-to-late stages of embryonic morphogenesis. In embryo representations, pharyngeal borders are indicated by black dashed lines; in cylindrical representations, the pharynx is represented by a spring that is attached to the anterior epidermis at the dark blue dot. Early comma, 1-5.fold and 3-fold stages of embryogenesis are depicted. Red arrows indicate the inward-pulling force on the epidermis that results from the resistance of the pharynx to stretching.

Figure 2. Genetic and phenotypic analyses support an extension spring model for pharyngeal elongation. (A–D) Predicted models and outcomes for testing the hypothesis that the elongating pharynx exerts an inward-pulling force on the anterior epidermis. Black arrows in models show the predicted (and observed) outcomes; gray arrows, alternative outcomes. For panels with DIC images, yellow dashed lines indicate lateral pharyngeal borders; orange dashed lines, the sensory depression or keyhole; black arrows, posterior extent of ingression. White scale bars = 10 μm. For additional details, see Table 1 and Supplementary File 1. (A) In *mec-8; pha-1(tm3671); sym-3* mutants that fail to establish a connection between the pharynx and epidermis (85%), deep ingressions or keyholes are not observed, whereas mutants that form an initial attachment (15%) form a stereotypical keyhole. (B) Detachment of the pharynx from the epidermis after the 2-fold stage in *mec-8; pha-1(e2123); sym-3* mutants leads to loss of the anterior ingression by the 3-fold embryonic stage and suppression of Pin in L1 larvae. (C) Whereas the depth of the keyhole in *mec-8; sym-4* mutants steadily increases between the 2- and 3-fold stages of embryogenesis, inhibition of embryonic elongation past the 2-fold stage by *let-502(RNAi)* prevents further deepening of the ingression. Error bars indicate 95% CIs, and diagrammed embryos denote the approximate stages of development for each genotype; n = 5 for each genotype at each time point. (D) Reversal of embryonic elongation in *mec-8; sqt-3(e2117ts)* mutants leads to a decrease in keyhole depth. Each line in the plot represents a different embryo; diagrammed embryos denote the approximate stages of development. For

these experiments, rare *mec-8; sqt-3(ts)* mutants that exhibited a keyhole at the 2-fold stage (~5%) were analyzed for reasons of experimental convenience.

Figure 3. Pharyngeal attachment leads to increased forces at sensory depression. A FRET-based TSMod inserted into the *C. elegans* β-spectrin gene (*unc-70*) was used to assess forces in live embryos. (A) Schematic for how UNC-70(TSMod) detects tension. FRET occurs when the donor fluorophore (mTFP) transfers energy to a nearby acceptor fluorophore (Venus) within the same peptide. When UNC-70(TSMod) experiences mechanical tension, a flexible linker separating mTFP and Venus is lengthened, leading to reduced FRET efficiency. (B–D) Representative images of wild-type and (F-H) *pha-1(tm3671)* strains that express UNC-70(TSMod). (J-L) Representative images of wild-type embryos expressing the no force control UNC-70(N-TSMod). Panels B,F,J depict 1.5-fold embryos after direct excitation of the Venus acceptor fluorophore. Panels C,D,G,H,K,L show FRET measurements where purple pixels indicate regions of highest tension (low FRET). Small white-framed boxes in panels B,C,F,G,J,K indicate the sensory depression region (SDR), which is enlarged in panels D,H,L. Red dashed lines in panels B,C,E,F,J,K outline the embryos. Scale bar in B = 30 μm. (E,I,M) FRET indices for the SDR and the region outside the sensory depression (Out-SDR). Individual embryos are represented by red circles, which are connected by lines to indicate values acquired from the same embryo. P-values depicted were calculated using a T-test (also see Supplementary File 2). Numbers at the bottom indicate the number of embryos that were analyzed for each condition. Each

point is an average of ~3-5 frames from a z-stack encompassing the embryo (see Methods for details).

Figure 4. Splicing between a subset of *fbn-1* exons is strongly misregulated in *mec-8* mutants. (A) A schematic of the *fbn-1* genomic locus is shown with alternatively spliced exons (e14-19) indicated by colored blocks and enlarged below. Single-sided arrows indicate PCR primers used in panel B. Lighter-shaded rectangles below exons 14 and 16 indicate alternative 3' splice sites for these exons. (B) PCR of the indicated regions of *fbn-1* using wild-type (N2) and *mec-8* cDNAs derived from embryos and wild-type genomic DNA (gDNA) as templates. White and black arrowheads indicate bands that correspond to known *fbn-1* isoforms (depicted on right) based on size estimations for PCR products (in basepairs): a/k = 476, b = 407, d = 341, e = 200, f = 248, g = 107, h = 182. Yellow arrowheads indicate aberrant *fbn-1* mRNA products that are present or are strongly enriched only in *mec-8* mutants. (C) Schematic of FBN-1 (a isoform) showing the locations of protein domains and the amino acid positions affected by *fbn-1* mutant alleles. For an annotated amino acid sequence, see Figure 4–figure supplement 2.

Figure 5. Morphogenesis defects of *fbn-1* mutants are strongly enhanced by mutations in *sym-3*, *sym-4* and *mec-8*. (A) RNAi feeding of *fbn-1* was carried out in the indicated backgrounds including strains hypersensitized to RNAi. Control RNAi strains contained the vector plasmid pPD129.36. (B) The Pin phenotype was scored in

fbn-1 mutant alleles and in selected double mutants with *fbn-1* and *mec-8*, *sym-3* or *sym-4*. Error bars in A and B represent 95% CIs. For additional information, see Table 1 and Supplementary File 1. (C) Representative images for select single and compound mutants. Note the presence of strong head malformations in *fbn-1(tm290); sym-3* and *fbn-1(tm290); sym-4* larvae. Also note that the strong epidermal malformations observed in *fbn-1(tm290); mec-8* mutants are suppressed by *let-502(RNAi)*. White arrows indicate ingressions or furrows throughout the epidermis; red arrows, detached anterior cells in *fbn-1(tm290); mec-8* mutants. Yellow dashed lines indicate lateral pharyngeal borders; orange dashed lines, the sensory depression or keyhole; black arrows, posterior extent of ingression. White scale bars = 10 μm.

Figure 6. The *fbn-1* gene is required in the epidermis and specifies a component of the embryonic sheath. (A) Systemic and epidermal-specific RNAi of *fbn-1* was carried out in wild-type (N2) and strain NR222, respectively, and in both backgrounds containing the *mec-8(u74)* allele. Note that both systemic and epidermal-specific *fbn-1(RNAi)* led to an increased percentage of Pin animals in the *mec-8* background. Error bars indicate 95% CIs; **P < 0.01. (B) Schematic of the *C. elegans* embryonic lineage and findings from the *fbn-1* mosaic analysis. Strains used for the analysis were WY1059, *fbn-1(tm290); sym-4(mn619); fdEx249[fbn-1(+); sur-5::GFP]*, and WY1068, *mec-8(u74); fbn-1(tm290); fdEx249*. Green numbers indicate the number of L4 or adult mosaic animals that were not Pin but contained the *fbn-1(+)* rescuing array within that lineage only. (C) Wild-type and *fbn-1(ns67)* embryos expressing P_{fbn-1}::GFP-PEST (a

convenient marker for embryonic epidermal cells). hyp4 cells within the focal plane are indicated and show aberrant morphologies in mutant embryos that contain a keyhole. (D). Expression of $P_{fbn\text{-}1}$::GFP-PEST and mini-*fbn-1*::mCherry (Δ*fbn-1*–49-2418) reporters. In the $P_{fbn\text{-}1}$::GFP-PEST panels, epidermal cells are indicated with white arrows. Black arrows indicate several cells positive for $P_{ttx\text{-}3}$::GFP, which was used as an injection marker and is not expressed in epidermal cells. In the mini-*fbn-1*::mCherry panels, the apical surface of embryonic epidermal cells (sheath) is indicated by white arrows. mini-*fbn-1*::mCherry is also detected in the extra-embryonic space (white dashed triangles). White scale bar = 10 μm, black bar = 5 μm.

Figure 7. The embryonic sheath is critical for resistance to biomechanical forces. (A) Wild-type embryos were treated with chitinase to remove part or all of the eggshell and then with trypsin to digest the sheath. Note the presence of a keyhole in both 2- and 3-fold trypsinized embryos (black arrows) and multiple ingressions or furrows in the epidermis of a 2-fold embryo (white arrowheads). Yellow dashed lines indicate lateral pharyngeal borders; orange dashed lines, the sensory depression or keyhole. White scale bars = 10 μm, black bars = 5 μm. (B) Model for the circumferential squeezing force (red arrows) and pharyngeal pulling force (yellow arrow) that act on the embryonic sheath. When the sheath is moderately weakened, such as when *fbn-1* function is partially impaired, a keyhole phenotype is observed, suggesting that the anterior epidermis is particularly sensitive to a reduction in sheath integrity as a result of the pharyngeal pulling force. In cases where the sheath is more severely compromised, the

depth of the keyhole may further increase, and the embryonic epidermis develops ingressions or furrows where circumferential constricting forces are acting.

Table 1. Ingression depths of the anterior epidermis

Genotype	Ingression depth (μm) ± 95% CI (range; n) 1.5-fold	3.0-fold
N2	2.12 · 0.23 (1.09–3.12; 20)	0.26 · 0.096 (0.0–0.67; 20)
sym-3(mn618)	2.39 · 0.40 (0.81–4.24; 24)	0.48 · 0.56 (0.0–6.55; 22)
sym-4(mn619)	2.74 · 0.64 (0.72–5.67; 21)	1.28 · 1.06 (0.0–6.74; 22)
mec-8(u74)	2.33 · 0.46 (0.72–4.34; 20)	2.42 · 1.50 (0.0–10.43; 26)
mec-8; sym-3[a]	4.25 · 0.89 (2.77–5.72; 18)	9.82 · 0.68 (7.84–12.00; 15)
mec-8; sym-4	4.27 · 1.16 (2.09–6.45; 16)	9.19 · 0.83 (7.07–10.14; 12)
pha-1(tm3671)	0.87 · 0.18 (0.45–1.18; 16)	NA
mec-8; pha-1(tm3671); sym-3[a]	0.83 □ 0.11 (0.40–1.19; 17)	NA
pha-1(e2123)	2.15 □ 0.27 (1.04–3.34; 19)	0.10 □ 0.07 (0.0–0.59; 16)
mec-8; pha-1(e2123); sym-3[a]	5.27 □ 0.53 (3.89–7.46; 14)	0.60 □ 2.35 (0.0–10.29; 19)
fbn-1(ns67)	3.18 □ 0.85 (0.60–6.02; 13)	5.34 □ 1.31 (0.0–9.24; 20)
fbn-1(ns67); sym-3	5.20 □ 0.41 (3.82–6.71; 20)	11.73 □ 0.85 (8.59–16.34; 19)
fbn-1(ns67); sym-4	5.98 □ 0.55 (4.25–7.66; 12)	12.84 □ 0.78 (9.65–16.37; 27)
mec-8; fbn-1(ns67)	5.03 □ 0.47 (3.76–7.19; 19)	9.84 □ 0.55 (6.94–12.24; 21)
fbn-1(tm290)	6.25 □ 1.81 (0.99–12.17; 16)	7.63 □ 3.66 (0.0–24.17; 17)
fbn-1(tm290); sym-3	5.65 □ 0.61 (2.59–7.29; 19)	15.05 □ 1.56 (9.12–26.06; 24)
fbn-1(tm290); sym-4	5.54 □ 0.86 (3.52–9.12; 17)	13.10 □ 1.72 (7.22–19.47; 20)

mec-8; fbn-1(tm290)	9.84 □ 0.55 (5.47–15.18; 31)	NA

[a]Because these strains give rise to a high frequency of viable *mnEx169*(–) progeny in the first generation following loss of the array (F1 escapers), next-generation progeny (F2) from *mnEx169(–)* F1 parents were scored. NA, Non-Applicable; these genotypes led to embryonic arrest prior to the 3-fold stage.

SUPPLEMENTARY DATA TITLES:

FIGURE SUPPLEMENTS

Figure 3–figure supplement 1. FRET index of low and high FRET controls. (A) Schematic of UNC-70(5aa) and UNC-70(TRAF) FRET controls. (B) Quantification of low (UNC-70(TRAF)) and high (UNC-70(5aa)) FRET controls in 1.5-fold embryos.

Figure 4–figure supplement 1. **Examples of gene regions differentially expressed in *mec-8* mutants and confirmed by RT-PCR.** Total RNA used for tilling arrays was reverse transcribed using oligo-dT primers and amplified by PCR using specific primers for each gene region (see Supplemental File 5). Each gene region was amplified using 30 cycles. Sizes are indicated in base pairs; arrows indicate bands that correspond to the expected sizes in mec-8 mutants based on tiling array results. For size reference, a 2-log DNA ladder (NEB) was used. (A) Control PCR with ama-1. (B) A gene (bed-2) with up-regulated introns (intron up) and that is not alternatively spliced (non-AS). (C) Intron up, AS gene (ZK180.5c and b). (D) Exon up, non-AS genes (hsp-16.41, F36A2.13, T15D6.8). (E) Exon up, AS genes (ajm-1, cah-4, ZK180.5a, asns-2). (F) Exon down, non-AS genes (C55B7.11, gcy-6, dmsr-14). (G) Exon down, AS gene (W05H9.1).

Figure 4–figure supplement 2. Amino Acid Sequence of FBN-1. Annotated peptide sequence for FBN-1 (a isoform). Locations of domains and genetic mutations are indicated.

SUPPLEMENTARY FILES

Supplementary File 1. Percentage of Pin Animals.

Supplementary File 2. Statistical analysis of FRET data.

Supplementary File 3. *mec-8* tiling array data.

Supplementary File 4. Figure legend for Supplementary File 3.

Supplementary File 5. Primer sequences for PCR.

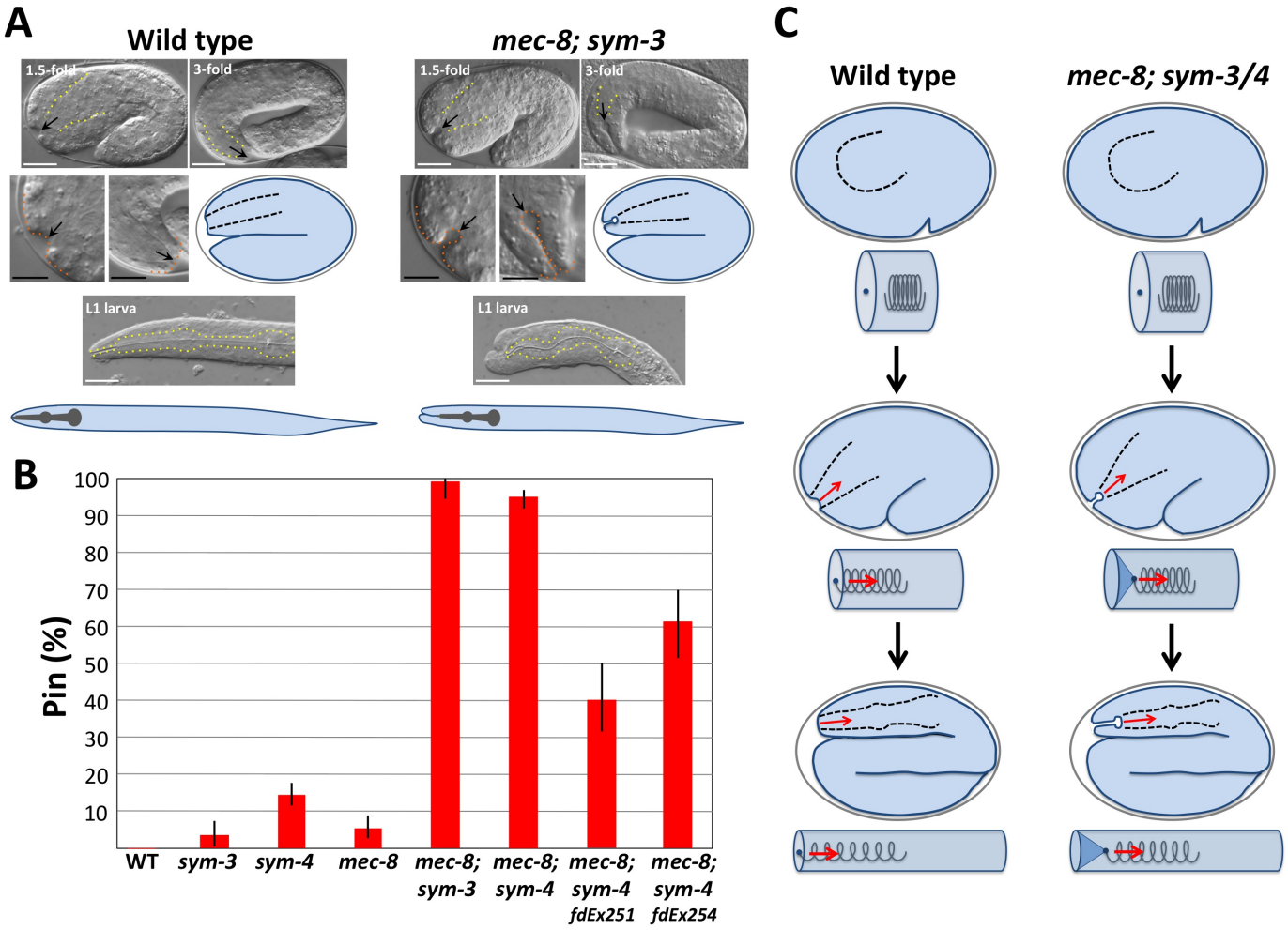
A
Wild type
mec-8; sym-3
1.5-fold
3-fold
1.5-fold
3-fold
L1 larva
L1 larva
B
Pin (%)
100
90
80
70
60
50
40
30
20
10
WT
sym-3
sym-4
mec-8
mec-8; sym-3
mec-8; sym-4
mec-8; sym-4 fdEx251
mec-8; sym-4 fdEx254
C
Wild type
mec-8; sym-3/4

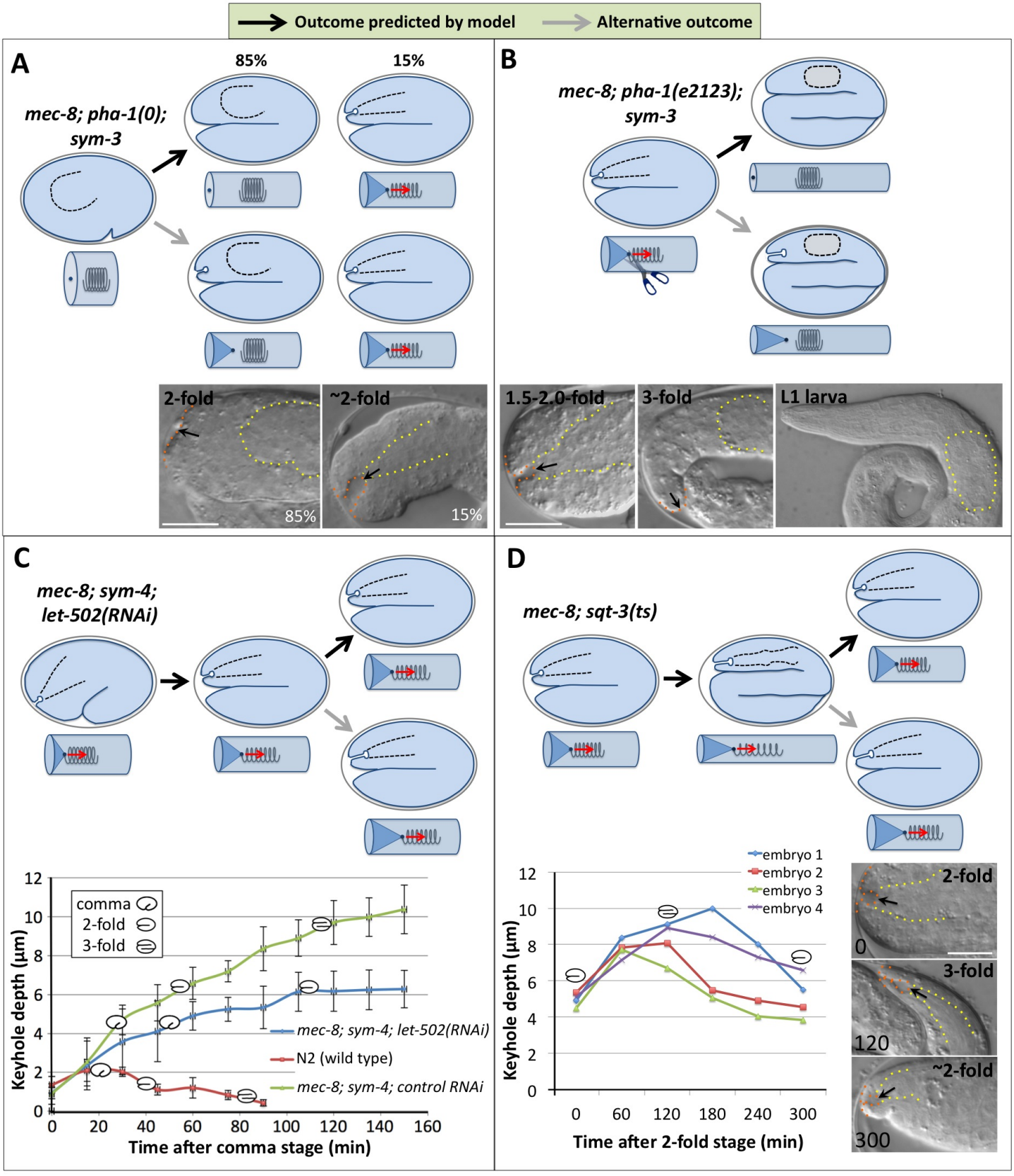
Outcome predicted by model
Alternative outcome
A
mec-8; pha-1(0); sym-3
85%
15%
2-fold
~2-fold
85%
15%
B
mec-8; pha-1(e2123); sym-3
1.5-2.0-fold
3-fold
L1 larva
C
mec-8; sym-4; let-502(RNAi)
comma
2-fold
3-fold
Keyhole depth (µm)
Time after comma stage (min)
mec-8; sym-4; let-502(RNAi)
N2 (wild type)
mec-8; sym-4; control RNAi
D
mec-8; sqt-3(ts)
embryo 1
embryo 2
embryo 3
embryo 4
Keyhole depth (µm)
Time after 2-fold stage (min)
2-fold
0
3-fold
120
~2-fold
300

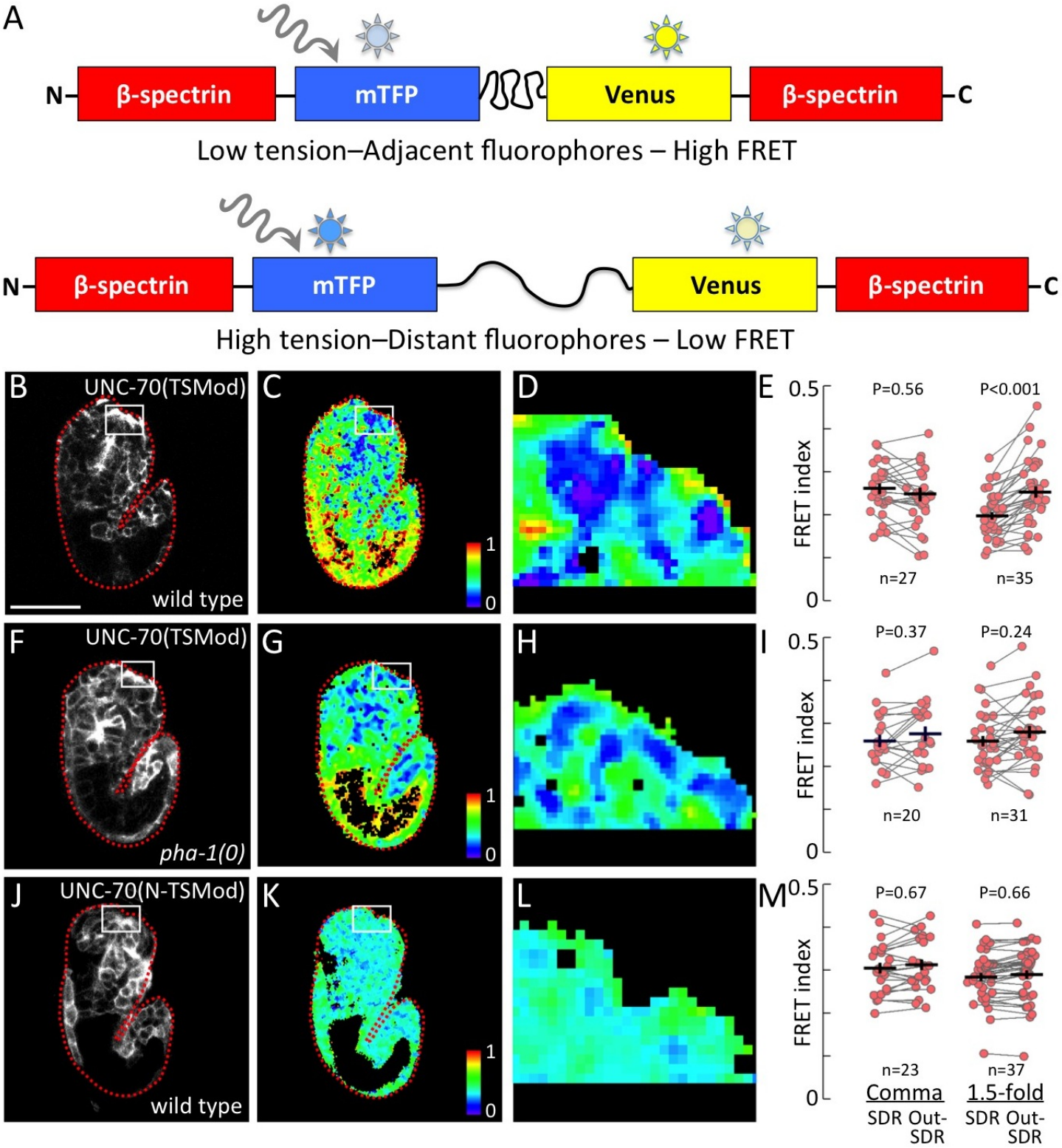
A
N
β-spectrin
mTFP
Venus
β-spectrin
C
Low tension–Adjacent fluorophores – High FRET
N
β-spectrin
mTFP
Venus
β-spectrin
C
High tension–Distant fluorophores – Low FRET
B
UNC-70(TSMod)
wild type
C
1
0
D
E
0.5
FRET index
0
P=0.56
P<0.001
n=27
n=35
F
UNC-70(TSMod)
pha-1(0)
G
1
0
H
I
0.5
FRET index
0
P=0.37
P=0.24
n=20
n=31
J
UNC-70(N-TSMod)
wild type
K
1
0
L
M
0.5
FRET index
0
P=0.67
P=0.66
n=23
n=37
Comma
1.5-fold
SDR Out-SDR
SDR Out-SDR

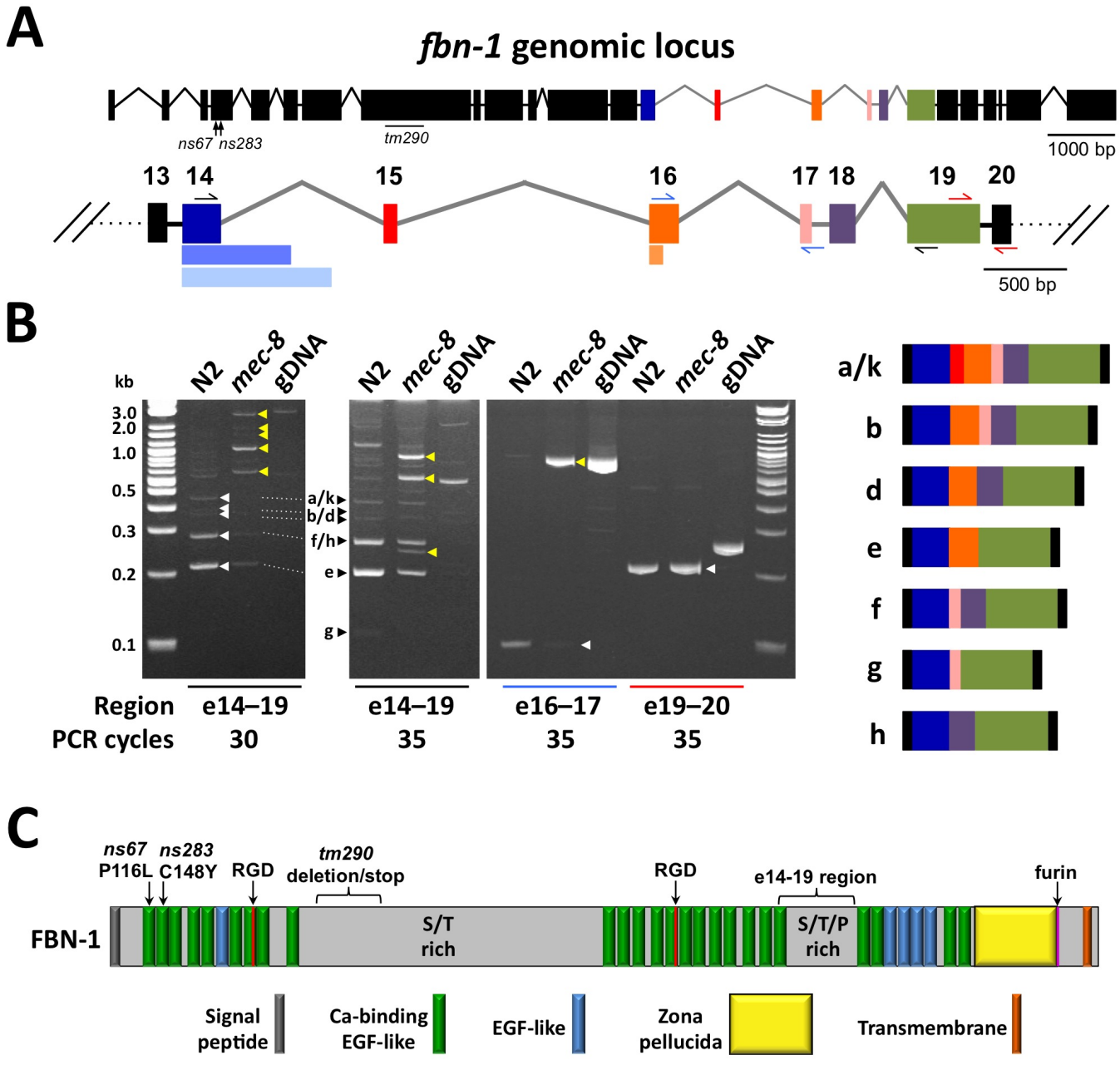
A
fbn-1 genomic locus
ns67 ns283
tm290
1000 bp
13 14 15 16 17 18 19 20
500 bp
B
kb
N2 mec-8 gDNA
3.0
2.0
1.0
0.5
0.3
0.2
0.1
a/k
b/d
f/h
e
g
Region e14–19 e14–19 e16–17 e19–20
PCR cycles 30 35 35 35
a/k
b
d
e
f
g
h
C
ns67 P116L
ns283 C148Y
RGD
tm290 deletion/stop
RGD
e14-19 region
furin
FBN-1
S/T rich
S/T/P rich
Signal peptide
Ca-binding EGF-like
EGF-like
Zona pellucida
Transmembrane

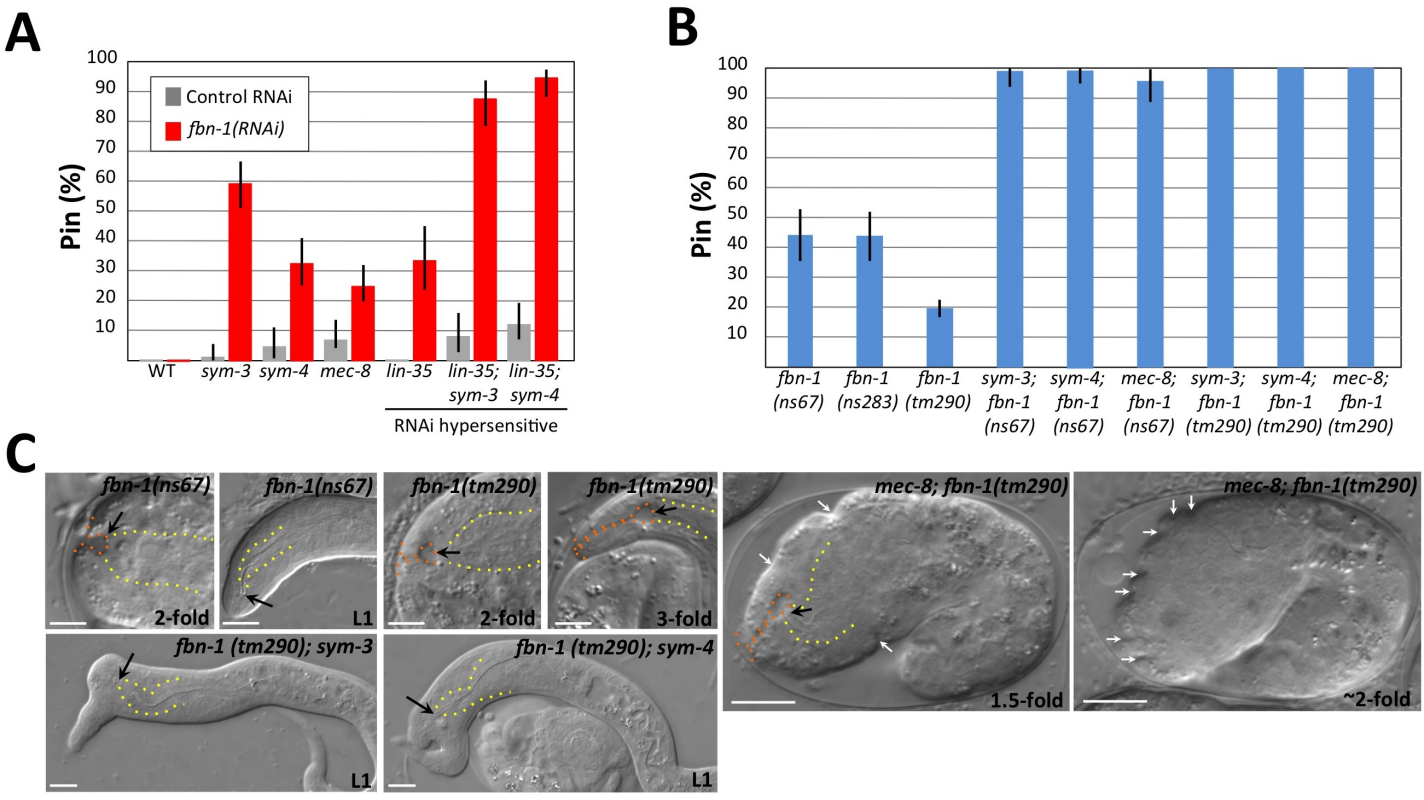
A
Pin (%)
Control RNAi
fbn-1(RNAi)
WT
sym-3
sym-4
mec-8
lin-35
lin-35; sym-3
lin-35; sym-4
RNAi hypersensitive
B
Pin (%)
fbn-1 (ns67)
fbn-1 (ns283)
fbn-1 (tm290)
sym-3; fbn-1 (ns67)
sym-4; fbn-1 (ns67)
mec-8; fbn-1 (ns67)
sym-3; fbn-1 (tm290)
sym-4; fbn-1 (tm290)
mec-8; fbn-1 (tm290)
C
fbn-1(ns67)
2-fold
fbn-1(ns67)
L1
fbn-1(tm290)
2-fold
fbn-1(tm290)
3-fold
mec-8; fbn-1(tm290)
1.5-fold
mec-8; fbn-1(tm290)
~2-fold
fbn-1 (tm290); sym-3
L1
fbn-1 (tm290); sym-4
L1

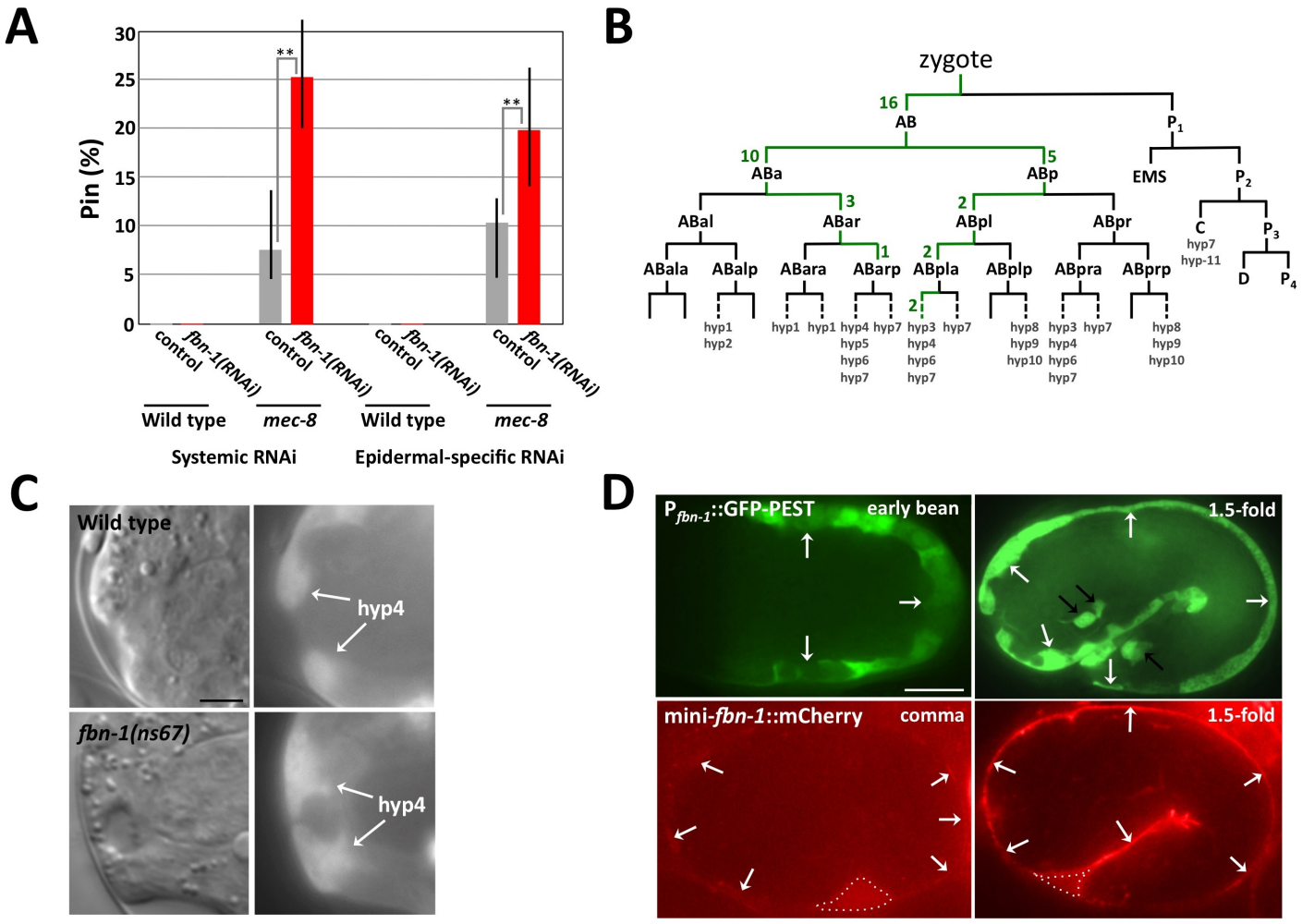
A
Pin (%)
30
25
20
15
10
5
0
**
**
control
fbn-1(RNAi)
control
fbn-1(RNAi)
control
fbn-1(RNAi)
control
fbn-1(RNAi)
Wild type
mec-8
Wild type
mec-8
Systemic RNAi
Epidermal-specific RNAi
B
zygote
16
AB
P1
10
ABa
5
ABp
EMS
P2
3
ABal
ABar
2
ABpl
ABpr
C
P3
hyp7
hyp-11
D
P4
1
2
2
ABala
ABalp
ABara
ABarp
ABpla
ABplp
ABpra
ABprp
hyp1
hyp2
hyp1
hyp1
hyp4
hyp7
hyp5
hyp6
hyp7
hyp3
hyp7
hyp4
hyp6
hyp7
hyp8
hyp9
hyp10
hyp3
hyp7
hyp4
hyp6
hyp7
hyp8
hyp9
hyp10
C
Wild type
hyp4
fbn-1(ns67)
hyp4
D
Pfbn-1::GFP-PEST
early bean
1.5-fold
mini-fbn-1::mCherry
comma
1.5-fold

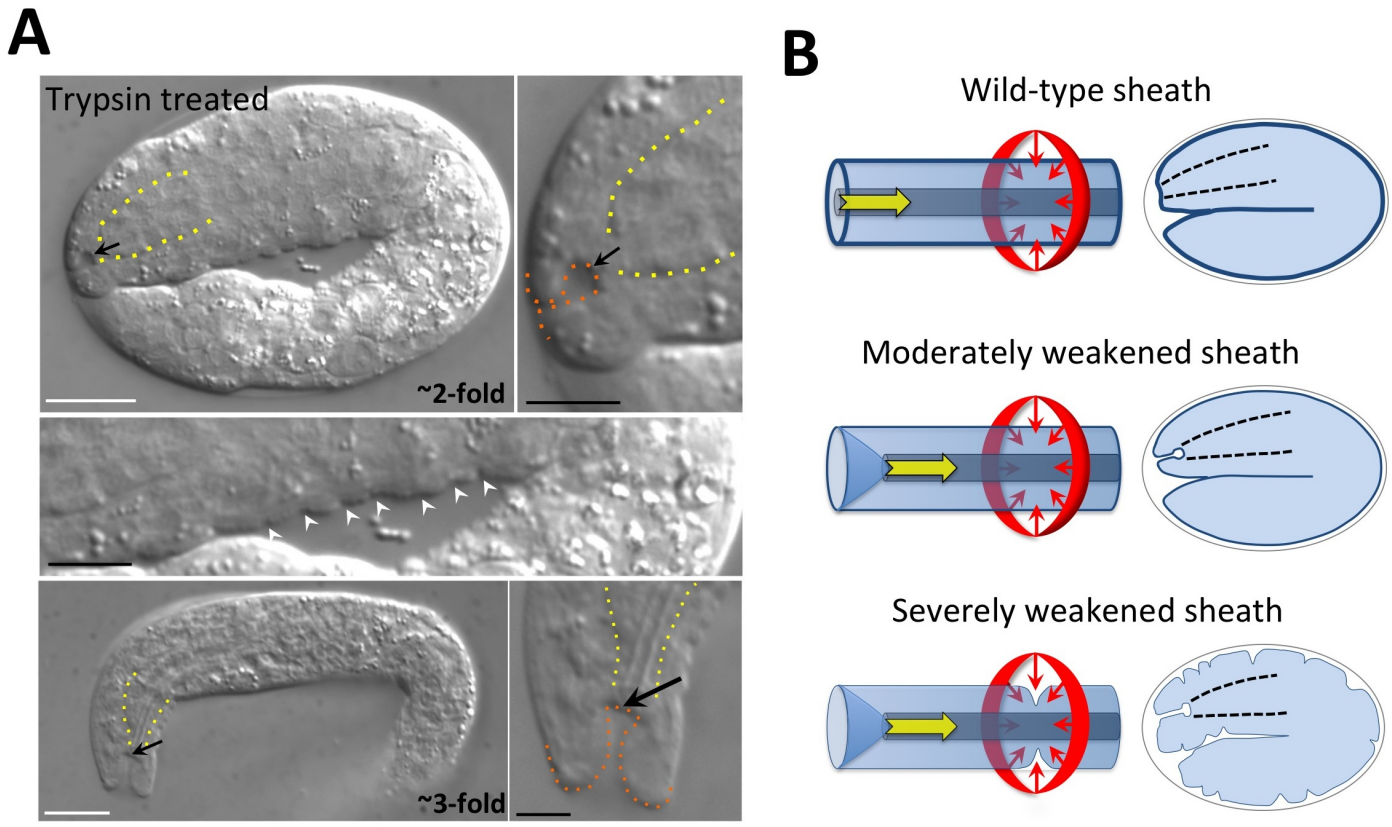
A
Trypsin treated
~2-fold
~3-fold
B
Wild-type sheath
Moderately weakened sheath
Severely weakened sheath